4 RELATIONSHIPS BETWEEN THE ELECTRICAL AND HYDROGEOLOGICAL PROPERTIES OF ROCKS AND SOILS

DAVID P. LESMES[1] and SHMULIK P. FRIEDMAN[2]

[1]*The George Washington University, Department of Earth and Environmental Sciences, Washington, D. C., U.S.A.*

[2]*Institute of Soil, Water, and Environmental Sciences, Agricultural Research Organization—The Volcanic Center, Bet Dagan, Israel*

4.1 Introduction

The ability to reliably predict the hydraulic properties of subsurface formations is one of the most important and challenging goals in hydrogeophysics. In water-saturated environments, estimation of subsurface porosity and hydraulic conductivity is often the primary objective. In partially saturated environments, characterization of the water content and the hydraulic conductivity as a function of saturation is also often required. Because the hydraulic conductivity of geologic formations varies by orders of magnitude over relatively small spatial scales, it is difficult to accurately characterize subsurface aquifer properties using just the information obtained from networks of widely spaced boreholes. A more complete and accurate characterization of the subsurface can be achieved by using an integrated exploration approach in which borehole and geophysical data sets are jointly interpreted. A key step in quantitative hydrogeophysical interpretations is the transformation of the measured geophysical properties into the desired hydrogeological parameters. This transformation typically relies on petrophysical relationships; these relationships can be developed at the field-scale using co-located hydrogeological-geophysical data, through laboratory experimentation on rock and soil samples, or by using theoretically based models. The objective of this chapter is to review the petrophysical models used to derive electrical-hydrogeological predictive relationships and to evaluate the theoretical and practical limitations of these relationships.

Electrical methods are widely used in hydrogeophysical investigations to obtain high-resolution information about subsurface conditions. These methods include electrical resistivity (ER), induced polarization (IP), electromagnetic induction (EMI), ground-penetrating radar (GPR), and time-domain reflectometery (TDR) surveys. These electrical methods, which operate at frequencies ranging from direct current (DC) to >1GHz, can be used individually or in combination to obtain information about the subsurface structure and composition. Both the structural information and the electrical property information provide important constraints for hydrogeological modeling. The structural information can be used to define hydrostratigraphic units as well as the locations of faults and fractures. The electrical property information can be used to qualitatively characterize the rock/soil type as well as the pore fluid properties. Petrophysical models can often be used to make more quantitative predictions about the

Y. Rubin and S.S. Hubbard (eds.), Hydrogeophysics, 87–128.

rock/soil properties, such as the water content, water conductivity, porosity, clay content, and hydraulic conductivity.

Petrophysical models of the electrical and hydrogeological properties of rocks and soils are formulated in terms of the intrinsic properties of the rock/soil system (i.e., the pore/grain topology and the physical and chemical properties of the pore fluids). Although the electrical and hydrogeological properties of rocks and soils depend on some common controlling factors, these relationships are often non-unique. As will be discussed in Chapter 17 of this volume, non-uniqueness can often be reduced by using multiple types of geophysical data or by applying other constraints based on a-priori information (e.g., pore fluid conductivity, porosity, and geological information). In practice, however, it is often difficult to constrain all of the model parameters required to make quantitative predictions. Therefore, theoretical models must either be simplified to reduce the number of free parameters, or empirical relationships can be established between the hydrogeological and electrical properties. These empirical relations are typically based on correlations made between electrical and hydrogeological measurements obtained from a specific site. These empirically established electrical-hydraulic relationships often work reasonably well; however, they are usually only applicable to the specific study site or to sites with similar characteristics (e.g., Huntley, 1986; Purvance and Andricevic, 2000).

We are therefore faced with the problem of the theoretically established electrical-hydrogeological petrophysical relationships being typically too complex (too many unconstrained parameters) to be applied in practice, and the empirically established relationships being valid only for specific sites. What we seek are theoretically based models that capture the intrinsic connections between the electrical and hydrogeolgoical properties, while being simple enough to be applied in the field. In this chapter, we review theoretically and empirically based models for the electrical prediction of hydrogeologic properties, and try to establish connections between these two approaches.

4.2 Hydrogeological and Electrical Properties

4.2.1 HYDROGEOLOGICAL PROPERTIES

Rocks and soils are composed of solid mineral grains and pore space. The porosity (n) is defined as the ratio of pore volume (V_p) to the total volume of the sample (V_t):

$$n = \frac{V_p}{V_t}. \tag{4.1}$$

Some materials contain isolated pores. In these cases, the effective porosity of the connected pore space is less than the total porosity.

4.2.1.1 *Saturated Flow*

The rate at which fluids flow through saturated porous materials is controlled by the saturated hydraulic conductivity (K_s). For homogeneous and isotropic materials, K_s is given by (e.g., Fetter, 2001)

$$K_s = \frac{k_s \rho_w g}{\mu}, \tag{4.2}$$

where k_s is the hydraulic permeability, μ is the fluid dynamic viscosity, ρ_w is the fluid density, and g is the acceleration of gravity. The hydraulic permeability is primarily a function of the pore size distribution, connectivity, and tortuosity of the pore network. In granular materials, the topology of the pore space is determined by the grain size distribution, the packing, and the cementation. Permeability models can either be formulated in terms of the characteristics of the pore space or in terms of the characteristics of the solid mineral grains (e.g., Nelson, 1994)

The equivalent channel model of Kozeny and Carman, or K-C (Carman, 1939), assumes that flow through a porous medium can be represented by flow through a bundle of capillaries. Each capillary is assumed to represent an independent flow path through the sample, where the effective path length (L_a) is greater than or equal to the macroscopic length of the sample (L). The tortuosity is defined as $T = (L_a/L)^2$. From considerations of laminar viscous flow through tubes, the following permeability equation is obtained (e.g., Scheidegger, 1974):

$$k_s = \frac{n r_h^2}{aT}, \tag{4.3}$$

where a is a tube shape factor (a dimensionless number between 1.7 and 3) and r_h is the hydraulic radius.

A common measure of the hydraulic radius is the reciprocal of the specific surface area (S_p), which is the ratio of pore surface area to pore volume. Furthermore, the tortuosity can be related to the electrical formation factor F (defined in Equation (4.26)) through the following relationship (e.g., Nelson, 1994)

$$T = \left(\frac{L_a}{L} \right)^2 = nF . \tag{4.4}$$

Equation (4.3) can then be expressed as

$$k_s = \frac{1}{aFS_p^2}. \tag{4.5}$$

This form of the K-C equation is more practical than Equation (4.3) because F and S_p are well-defined physical properties that can be measured, whereas T and r_h are theoretical constructs that cannot be directly measured.

Grain-based permeability models predict k_s to be dependent on the square of an effective grain size. In the Hazen model, the hydraulic conductivity is given by (e.g., Fetter, 2001)

$$K_s = Cd_{10}^2, \tag{4.6}$$

where the effective grain size d_{10} (in cm) corresponds to the grain size for which 10% of the sample is finer, and the coefficient C depends upon the grain sorting. The Hazen model is applicable to sediments where d_{10} ranges between 0.1 and 3.0 mm. More elaborate grain-based permeability models explicitly account for the effects of grain sorting and porosity (e.g., Nelson, 1994).

4.2.1.2 *Unsaturated Flow*

In the unsaturated zone, the pore space is filled with water and air, and the water is held in tension (negative pressure). The water saturation (S) is the ratio of the volume of water (V_w) to the total pore volume:

$$S = \frac{V_w}{V_p} . \tag{4.7}$$

The water content (θ) is defined as the ratio of the volume of water to the total volume of the sample:

$$\theta = \frac{V_w}{V_t} . \tag{4.8}$$

The hydraulic conductivity of partially saturated rocks and soils (K) is a function of K_s as well as the saturation level and the soil-moisture-retention properties of the material.

The soil-moisture-retention function $\theta(\psi)$ describes the relationship between the water content and the capillary head (ψ). For a capillary tube of radius r, the capillary head is given by

$$\psi = -2\gamma \cos\beta / \rho_w g r \tag{4.9}$$

where γ is the surface tension between water and air, and β is the contact angle. The shape of the soil-moisture-retention function is primarily controlled by the pore size distribution, as large pores tend to drain at low pressures and increasingly smaller pores drain at higher pressures (e.g., Fetter, 2001). Many empirical and theoretical models have been developed to fit soil-moisture-retention measurements. The most widely used function is that developed by van Genuchten (1980). The effective saturation (S_e) for the van Genuchten function is given by

$$S_e = \frac{\theta - \theta_r}{\theta_s - \theta_r} = \frac{1}{\left[1 + \alpha(\psi)^n\right]^m} \tag{4.10}$$

where θ_s and θ_r are the saturated and residual water contents, respectively, and α, m, and n are fitting parameters, which can be related to the statistics of the pore size distribution function (e.g., Kosugi, 1994).

The relative hydraulic conductivity ($K_r = K/K_s$) decreases with decreasing saturation, as under these conditions, pore water is held more tightly, and the fluid must take a more tortuous flow path as the larger pores drain. The dependence of K_r on θ is determined by the soil-moisture-retention function (e.g., Fetter, 2001). Mualem's (1976) model for predicting K_r from the soil-water-retention function is

$$K_r = K / K_s = S_e^{1/2} \left\{ \int_0^{S_e} \frac{dS_e}{|\psi|} \Big/ \int_0^1 \frac{dS_e}{|\psi|} \right\}^2 . \tag{4.11}$$

To predict K_r using Equation (4.11), one must specify $S_e(\psi)$. As described above, K_s can be predicted from measurements of F, and an effective pore or grain size. $S_e(\psi)$ can be predicted from the pore size distribution of the sample (e.g., Kosugi, 1994). Therefore, if the formation factor and the pore-size distribution of a rock or soil sample are known, it should be possible to make relatively accurate estimates of the saturated and unsaturated hydraulic properties of the sample (i.e., K_s, $S_e(\psi)$ and K_r). In the rest of this chapter, we address the feasibility of electrically estimating the key rock and soil properties required to predict flow in subsurface formations.

4.2.2 ELECTRICAL PROPERTIES

The conductive and capacitive properties of a material can be represented by a complex conductivity (σ^*), a complex resistivity (ρ^*), or a complex permittivity (ε^*), where

$$\sigma^* = \frac{1}{\rho^*} = i\omega\varepsilon^* \tag{4.12}$$

and ω is the angular frequency ($\omega = 2\pi f$) and $i = \sqrt{-1}$ (e.g., Schön, 1996). The complex electrical parameters can be expressed either in polar or rectangular form. For example, the complex conductivity can be expressed in terms of a magnitude ($|\sigma|$) and phase (ϕ), or by real (σ') and imaginary (σ'') components:

$$\sigma^* = |\sigma| e^{i\phi} = \sigma' + i\sigma'' . \tag{4.13}$$

The complex conductivity response of Berea sandstone saturated with 0.01M KCl and measured over the frequency range of 10^{-3} Hz to 10^6 Hz is plotted in Figure 4.1. Also plotted in Figure 4.1 is the real part of the relative permittivity or dielectric constant. The dielectric constant (κ') is the ratio of the permittivity of the sample (ε') to the permittivity of vacuum (ε_0), and it is proportional to the imaginary component of the complex conductivity

$$\kappa' = \frac{\varepsilon'}{\varepsilon_0} = \frac{\sigma''}{\omega\varepsilon_0} . \tag{4.14}$$

As the dielectric response approaches the low-frequency limit (κ'_{static}), the imaginary conductivity goes to zero. As the dielectric response approaches the high-frequency limit (κ'_∞), the imaginary conductivity becomes large.

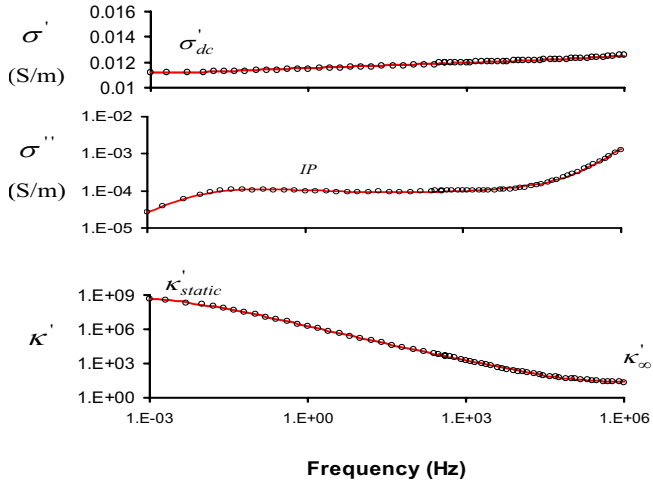

Figure 4.1. Complex responses of Berea sandstone saturated with 0.01 M NaCl (Lesmes and Frye, 2001): (top) real component of complex conductivity, (middle) imaginary component of complex conductivity, (bottom) dielectric constant or permittivity

In the laboratory, three different measurement systems are needed to measure the broadband electrical impedance response from 10^{-3} Hz to 10^{9} Hz. Four electrode systems are used to measure the impedance response from 10^{-3} Hz to 10^{3} Hz; two-electrode systems are used to measure the impedance response from 10^{2} Hz to 10^{7} Hz; and transmission line systems (e.g., TDR) are used to measure the impedance response from 10^{6} Hz to 10^{10} Hz (Olhoeft, 1985, 1986). The effective frequency range of each of these measurement systems is limited by systematic errors intrinsic to the measurement configuration. For each measurement system, it is possible to have large systematic errors that are stable and repeatable but give erroneous results. It is important, therefore, to test and calibrate these systems with known standards (e.g., standard resistors and standard brines) to determine the overall accuracy and precision of the measurements (Olhoeft, 1985; VanHalla and Soinenen, 1995; Lesmes and Frye, 2001). It is not possible to measure the complete broadband impedance response in the field with currently available instrumentation. As with laboratory measurement systems, theoretical and practical considerations limit the effective frequency ranges of the various electrical geophysical instruments and methods. The most commonly measured electrical parameters in the field are the high-frequency permittivity or dielectric constant (κ'_{∞}), the low-frequency conductivity (σ'_{dc}), and a low-frequency capacitance, commonly referred to as the induced polarization (IP) or complex resistivity (CR) response. These electrical parameters can be directly measured with point sensors or indirectly estimated by inverting noninvasive geophysical measurements for the subsurface electrical properties. Dielectric measurements are typically made using TDR (refer to Chapter 15 of this volume) or GPR methods (Chapter 7), and conductivity measurements are typically made using electrical resistivity (Chapter 5) or electromagnetic induction methods (Chapter 6). The IP and CR methods are similar to the electrical resistivity method, but they measure both the low-frequency conductive and capacitive properties of a material (see Chapter 5).

The three electrical parameters—κ'_∞, σ'_{dc}, and an IP parameter (there are several different but equivalent measures of the IP response)—contain complementary information about a material. Petrophysical models can be used to interpret these electrical measurements in terms of the physical and chemical properties of a material. Models for the high-frequency dielectric response (κ'_∞) and the low-frequency conductivity response (σ'_{dc}) of rocks and soils are reviewed below in Sections 4.3 and 4.4, respectively. Models for the induced polarization response and the frequency-dependent complex conductivity response of rocks and soils are reviewed below in Sections 4.5 and 4.6, respectively.

4.3 Permittivity Models

In this section, we review models for the frequency-independent permittivity responses of rocks and soils. These models are generally applicable to permittivity measurements made in the frequency range of 100 MHz to 10 GHz. At lower frequencies, polarization mechanisms cause the permittivity responses of rocks and soils to increase with decreasing frequency (see Figure 4.1). At very high frequencies (f >10 GHz), the permittivity begins to decrease as the relaxation frequency of water molecules is approached. The high-frequency limit of the permittivity response, indicated as κ'_∞ in Figure 4.1, is referred to as κ_{eff} in the models presented in this section. The high-frequency permittivity response of rocks and soils is primarily sensitive to the water content, as the relative permittivity of water, $\kappa_w \cong 80$, is much higher than the relative permittivity of dry mineral grains, κ_s = 4 to 8, or air, κ_a = 1 (e.g., Olhoeft, 1981). Secondary factors affecting the permittivity responses of rocks and soils include the effective shapes of the pores and grains, fine-scale laminations, temperature, and to a lesser degree the salinity of the saturating solution (e.g., Olhoeft, 1981; Schön, 1996). Models of the high-frequency permittivity responses of rocks and soils are generally not dependent upon the pore or grain size. As discussed at the end of this section, some attempts have been made to predict the hydraulic conductivity of earth materials from high-frequency permittivity measurements. However, it is not possible to theoretically derive a predictive relationship between permittivity and hydraulic conductivity, so the empirically obtained relationships are quite site specific.

4.3.1 WATER-SATURATED MEDIA

The refractive index (RI) model (Birchak et al., 1974) is the most widely used relationship to predict the relative volume fractions of two-phase mixtures. For water-saturated porous materials, the RI model is given by

$$\sqrt{\kappa_{eff}} = n\sqrt{\kappa_w} + (1-n)\sqrt{\kappa_s} \quad . \tag{4.15}$$

By specifying κ_W and $\kappa_{S,,}$ the RI model can be used to predict the porosity of water - saturated materials from their measured permittivity. The physical assumption behind

the RI model is that the time for an EM wave to travel through a porous material is equal to the sum of the travel times for it to pass through the separate phases of the material (solid grains and pore water) as if they were arranged in series. Equation (4.15) is also referred to as the CRIM equation or the time propagation equation (Wharton et al., 1980). The slight decrease in κ_w with increasing temperature and salinity can be computed using Equations 4.68 and 4.69, respectively, given in the Appendix.

The dielectric constant κ_s of common rock and soil-forming minerals is much smaller that the dielectric constant of water—for example: quartz $\cong 4.5$, calcite $\cong 9$, and clay $\cong 5.5$ (Robinson and Friedman, 2003; Robinson, 2004). For mixtures of different types of mineral grains, the dielectric constant of the solid matrix can be estimated as the weighted arithmetic mean of the dielectric constants for the different mineral constituents (Robinson and Friedman, 2002).

Theoretically based models can be used to predict the dielectric properties of heterogeneous materials in terms of the permittivities and volume fractions of the individual phases and their microgeometrical configurations. Continuum mean field theories are widely used to predict the dielectric and conductive properties of rocks and soils. The following "universal" mixing formula can be used to represent several dielectric mixing models derived using different mean-field theory approaches (Sihvola and Kong, 1988, 1989):

$$\kappa_{eff} = \kappa_w + \frac{\left[\dfrac{(1-n)(\kappa_s-\kappa_w)\left[\kappa_w + a(\kappa_{eff}-\kappa_w)\right]}{\left[\kappa_w + a(\kappa_{eff}-\kappa_w) + \dfrac{1}{3}(\kappa_s-\kappa_w)\right]}\right]}{\left[1 - \dfrac{\dfrac{1}{3}(1-n)(\kappa_s-\kappa_w)}{\left[\kappa_w + a(\kappa_{eff}-\kappa_w) + \dfrac{1}{3}(\kappa_s-\kappa_w)\right]}\right]}. \tag{4.16}$$

Equation (4.16) expresses the effective dielectric constant as a function of a background phase of the pore solution (with relative permittivity κ_w and volume fraction n), with spherical inclusions of the mineral grains (relative permittivity κ_S and volume fraction 1-n). The heuristic parameter a in Equation (4.16), which ranges from 0 to 1, accounts for the effect of neighboring particles on the internal electrical field of a reference particle. The term ($\kappa_w + a(\kappa_{eff} - \kappa_w)$) in this equation represents the apparent permittivity of the background as felt by a reference particle. When there are no interactions between the embedded particles, the heuristic parameter $a = 0$ and the universal mixing formula reduces to the Maxwell-Garnett (MG) model (Maxwell and Garnett, 1904), which can be expressed as

$$\kappa_{eff} = \kappa_w + 3(1-n)\kappa_w \frac{\kappa_s - \kappa_w}{\kappa_s + 2\kappa_w - (1-n)(\kappa_s - \kappa_w)}. \tag{4.17}$$

The MG model results in an upper bound for the permittivity response of a water-saturated sample. When $a = 2/3$, the universal mixing formula results in the symmetric

effective-medium approximation (Polder and van Santen, 1946) (PVS model); and when a=1, it results in the coherent potential (CP) mixing formula (Tsang et al., 1985). The PVS and CP mixing formulas account for interactions between the embedded particles; they usually underpredict the permittivity responses of high-porosity granular materials such as soils (Jones and Friedman, 2000). To account for modest interactions between the embedded particles Friedman and Robinson (2002) set a = 0.2 in Equation (4.16) and obtained good fits to permittivity measurements made on water-saturated packings of glass beads, quartz sand, and tuff grains.

The mean-field theories expressed in Equations (4.16) and (4.17) are for spherical inclusions; however, pore/grain shape significantly affects the permittivity response of porous materials. In effective media theories, the particle shape is typically represented by an ellipsoid of revolution (spheroid) for which analytical expressions can be derived (e.g., Sihvola and Kong, 1988; Jones and Friedman, 2000). By extending or contracting the b and c axes while keeping a constant, a sphere can be transformed into either disk-like (oblate) particles or needle-shaped (prolate) particles. The effect of particle shape and orientation on the permittivity response is characterized by the depolarization factors: N^a, N^b, and N^c. For ellipsoids of revolution, where $a \neq b = c$, Jones and Friedman (2000) found that $N^a(a/b)$ is well approximated by a single empirical expression (r^2 = 0.9999):

$$N^a = \frac{1}{1+1.6(a/b)+0.4(a/b)^2} \quad ; \quad N^b = N^c = \frac{1}{2}(1-N^a) \,. \tag{4.18}$$

The depolarization factors for a sphere (a/b=1) are $N^{a,b,c}$ = 1/3, 1/3, 1/3; for a thin disk (a/b<<1) $N^{a,b,c}$ =1,0,0; and for a long needle (a/b>>1) $N^{a,b,c}$=0, 1/2, 1/2.

Nonspherical particles can form either anisotropic or isotropic packings, depending on whether the particles are aligned or randomly oriented. The effective permittivity of a material composed of nonspherical particles, aligned to make a uniaxial-anisotropic medium, is described by a second-order tensor with diagonal components given by $\kappa_{eff}^{\ a} \neq \kappa_{eff}^{\ b} = \kappa_{eff}^{\ c}$. The effective permittivity in the ith direction takes the form (Sihvola and Kong, 1988):

$$\kappa_{eff}^{\ i} = \kappa_w + \frac{\dfrac{(1-n)[\kappa_w + a(\kappa_{eff}^{\ i} - \kappa_w)](\kappa_s - \kappa_w)}{\kappa_w + a(\kappa_{eff}^{\ i} - \kappa_w) + N^i(\kappa_s - \kappa_w)}}{1 - \dfrac{(1-n)N^i(\kappa_s - \kappa_w)}{\kappa_w + a(\kappa_{eff}^{\ i} - \kappa_w) + N^i(\kappa_s - \kappa_w)}} \tag{4.19}$$

where the depolarization factors (N^i) are defined by the particle aspect ratio according to Equation (4.18). Nonspherical particles that are randomly oriented form an isotropic medium with a scalar effective permittivity given by (Sihvola and Kong,1988):

$$\kappa_{eff} = \kappa_w + \frac{\sum_{i=a,b,c} \frac{(1-n)[\kappa_w + a(\kappa_{eff} - \kappa_w)](\kappa_s - \kappa_w)}{3[\kappa_w + a(\kappa_{eff} - \kappa_w) + N^i(\kappa_s - \kappa_w)]}}{1 - \sum_{i=a,b,c} \frac{(1-n)N^i(\kappa_s - \kappa_w)}{3[\kappa_w + a(\kappa_{eff} - \kappa_w) + N^i(\kappa_s - \kappa_w)]}} \tag{4.20}$$

The MG model formed the basis of a self-similar (SS) model derived by Bruggeman (1935) for spheres and generalized to ellipsoids by Sen et al. (1981), in which the solid-phase inclusions were sequentially added to the host water phase, while the background pore system remained intact to low values of porosity. The resulting formula is impressively simple (Sen et al., 1981):

$$\left(\frac{\kappa_s - \kappa_{eff}^i}{\kappa_s - \kappa_w}\right)\left(\frac{\kappa_w}{\kappa_{eff}^i}\right)^{N^i} = n, \tag{4.21}$$

where the depolarization factors can again be computed using Equation (4.18). This model applies, in principle, to a fractal medium of infinitely wide particle size distribution and therefore forms a lower bound for the estimate of κ_{eff}^i of water-saturated porous media (Robinson and Friedman, 2001). An isotropic form of the SS model can be obtained by averaging the depolarization factors (N^i) over all possible particle orientations (Mendelson and Cohen, 1982). The isotropic form of the SS model can be expressed as

$$\kappa_{eff} = \kappa_w n^m \left(\frac{1 - \kappa_s / \kappa_w}{1 - \kappa_s / \kappa_{eff}}\right)^m, \tag{4.22}$$

where the effective cementation exponent m is a function of the particle shape (Mendelson and Cohen, 1982), with an arithmatic correction by Sen (1984):

$$m = \left\langle \frac{(5 - 3N)}{3(1 - N^2)} \right\rangle. \tag{4.23}$$

As will be described in Section 4.4, this cementation exponent m can also be used to describe the effects of cementation and grain shape on the conductivity response of rocks and soils (e.g., Equations (4.26) and (4.35)). For high-porosity granular materials such as soils, we typically set m=1.5, and for consolidated rocks with lower porosity, we typically use a cementation exponent of m=2.0 (Sen et al., 1981; Mendelson and Cohen, 1982; Sen, 1984; Robinson and Friedman, 2001).

The relative permittivity responses of isotropic materials computed using the RI, MG, and SS models with κ_W =80 and κ_S = 5 are plotted as a function of porosity in Figure 4.2. The MG and SS model responses are computed for both spherical particles (a/b=

1.0, N^a=1/3, m=1.5) and oblate particles with random orientations (a/b= 0.22, N^a=0.73, m=2.0). As shown in Figure 4.2, the permittivity responses of all the models increase with increasing porosity. As previously discussed, the MG and SS models give realistic upper and lower bounds, respectively, for the permittivity responses of earth materials. The MG and SS models with randomly oriented oblate grains give smaller permittivity responses than the spherical grain models. The response of the RI model is similar to the responses predicted by the SS model with spherical grains and the MG model with oblate grains. Porosity predictions made using these three models differ by less than 0.03 porosity units over the porosity range of 0 to 0.5, thus illustrating the practicality of the RI model.

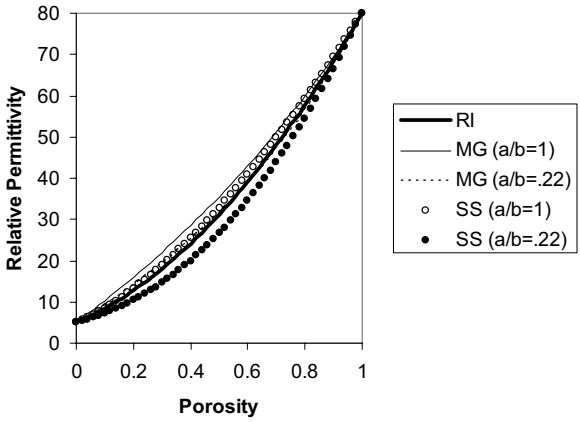

Figure 4.2. Relative permittivity responses of a water-saturated media ($\kappa_w = 80$; $\kappa_s = 5$) predicted by the refractive index (RI) model, the Maxwell-Garnett (MG) model, and the self-similar (SS) model. The aspect ratios of the spherical (a/b=1) and oblate (a/b=0.22) particle inclusions used in the MG and SS model calculations are indicated in the figure legend. An aspect ratio of a/b=0.22 corresponds to a cementation exponent of m=2.0. Note that the MG (a/b=0.22) curve is not visible because it is very similar to, and overlaid by, the SS (a/b=1) and the RI responses.

The effects of particle shape on the relative permittivity responses of the MG and SS models are further illustrated in Figure 4.3. In this plot, the relative permittivity is computed for n=0.3 and plotted as a function of the aspect ratio (a/b) for the MG and SS models. The solid lines refer to the MG model computations and the dashed lines refer to the SS model computations for κ_{eff}^{a}, κ_{eff}^{b}, and the isotropic mixture of randomly oriented particles κ_{eff}. The κ_{eff}^{a} and κ_{eff}^{b} responses for the anisotropic MG and SS models approach the same limiting values for very oblate and very prolate particle shapes. The κ_{eff}^{a} responses are maximum for long needle-like particles (a/b=10^3), and the κ_{eff}^{b} responses are maximum for thin disk-like particles (a/b=10^{-3}). The MG and SS model responses for randomly oriented particles have similar dependencies upon the particle shape, except that the SS model response, which takes into account particle interactions, is shifted approximately 3 permittivity units lower than the response of the MG model.

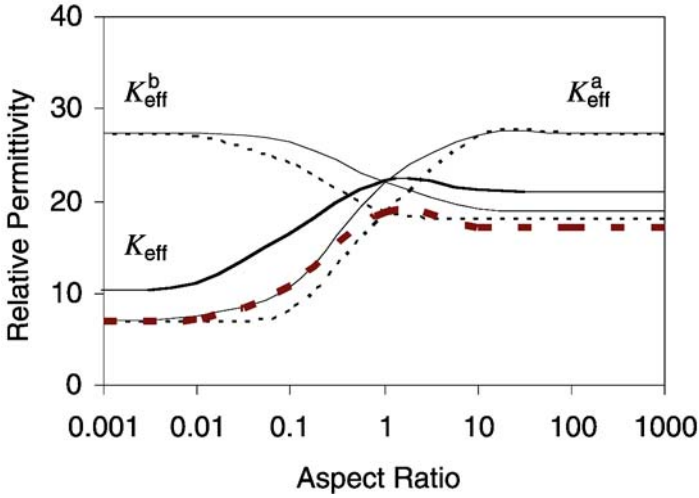

Figure 4.3. Relative permittivity of water saturated media ($\kappa_w = 80$; $\kappa_s = 5$; n= 0.3) computed using the MG model (solid lines) and the SS model (dashed lines). The orientations of the particles relative to the applied fields (κ_{eff}^{a} and κ_{eff}^{b}) are indicated on the plot. The bold solid and bold dashed lines are the MG and SS model responses, respectively, for randomly oriented particles κ_{eff} .

4.3.2 UNSATURATED MEDIA

The refractive index model (Equation 4.15) can be extended to model the effective permittivity of three-phase mixtures (e.g., Alharthi and Lange, 1987)

$$\sqrt{\kappa_{eff}} = \theta\sqrt{\kappa_w} + (n-\theta)\sqrt{\kappa_a} + (1-n)\sqrt{\kappa_s} \quad . \tag{4.24}$$

Several further modifications of Equation (4.24) have been proposed, such as splitting the solid phase into sand and clay phases of different permittivities (Wharton et al., 1980; Knoll et al., 1995), or replacing the ½ exponent with different powers (Loyenga, 1965; Roth et al., 1990). However, to predict water content from permittivity measurements using Equation (4.24), the porosity of the material must be specified in addition to the permittivities of the individual phases. Since the porosity of soil and rock formations is variable and often unknown, several empirical equations have been developed to directly predict the relationship between κ_{eff} and θ (Topp et al., 1980; Wang and Schmugge, 1980; Roth et al., 1992). Most of these empirical relationships use polynomial functions, which in some cases account for soil textural parameters such as the clay and sand percentage (Dobson et al., 1984) or the bulk density and clay and organic matter contents (Jacobsen and Schjonning, 1993). The most reliable and widely used $\kappa_{eff}(\theta)$ relationship for soils is the empirical formula of Topp et al. (1980):

$$\kappa_{eff} = 3.03 + 9.3\theta + 146\theta^2 - 76.7\theta^3 , \tag{4.25}$$

which was best-fitted to careful measurements made on four soil types and was suggested to hold approximately for all types of mineral soils. This relationship was found to give good predictions for coarse and medium-textured soils (Dirksen and

Dasberg, 1993; Friedman, 1998a), and gives similar predictions for several theoretically derived models (Friedman, 1997, 1998a).

The permittivity responses of the Topp model and the three-phase RI model with n=0.5 are plotted in Figure 4.4. The Topp and R.I. equations work well for coarse and medium-textured soils (Dirksen and Dasberg, 1993; Friedman, 1998a). However, they do not work as well for fine textured soils. The presence of soil minerals affects the dielectric properties of the water molecules adjacent to their surfaces by restricting their rotational movements, thus reducing their polarizability and permittivity (e.g., Dobson et al., 1985; Dirksen and Dasberg, 1993; Heimovaara et al., 1994; Or and Wraith, 1999). In these cases, the Topp and RI equations underpredict the water content of fine-textured soils. This effect can be accounted for in $\kappa_{eff}(\theta)$ models by adding a fourth, bound water phase with a permittivity similar to that of ice κ_{bw}=3.5 (Dobson et al., 1985; Dirksen and Dasberg, 1993), or by varying continuously κ_w as a function of the mean thickness of the water films surrounding the soil particles (Friedman, 1998a).

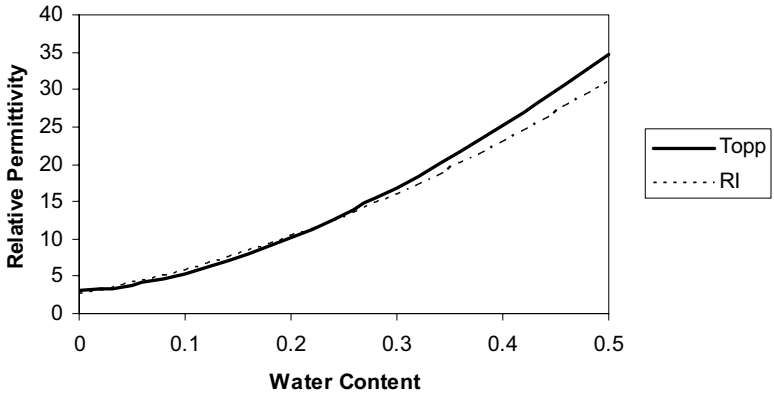

Figure 4.4. Relative permittivity of an unsaturated medium (n=0.5) computed using the the three-phase refractive index model ($\kappa_w = 80$; $\kappa_s = 5$) and the Topp et al (1980) equation

For permittivity measurements made at frequencies <100 MHz, the surface polarization of fine-textured soils can cause large enhancements in the permittivity response. In these cases, the Topp and RI equations overpredict the water content of fine-textured rocks and soils. Four-phase mixing formulae can also be used to account for clay polarization effects (Knoll et al., 1995); however, the permittivity responses of clay can be much larger than the permittivity response of water, and the clay response varies with clay type, water conductivity, and temperature. Therefore, it is difficult to accurately account for the clay polarization effects in lower-frequency permittivity estimates of water content.

Theoretically based effective medium models can be used to better understand the geometric factors controlling the permittivity responses of partially saturated rocks and soils. For example, Friedman (1998a) developed a MG-type three-phase mixing model consisting of concentric spheres of grains, water, and air. There are six possible

concentric arrangements of the three phases, and because the permittivity of water is much higher than that of the other phases, it is primarily the location of the water phase that dictates the resulting κ_{eff}. In order to use theoretically derived models to predict water content from permittivity measurements, the model parameters must be measured or their values assumed to be known. For this reason, most practical applications use models calibrated with site-specific data or (more commonly) empirical formulae such as the Topp equation, which are based on fits to laboratory measurements.

4.3.3 PERMEABILITY PREDICTION

Both k_s and κ_{eff} depend on porosity and the effective pore/grain shapes of earth materials. Therefore, permittivity measurements could possibly be used to constrain these parameters in a permeability prediction formula (e.g., Equation 4.3). However, k_s is also strongly dependent upon the pore/grain size, which cannot be determined from high-frequency permittivity measurements. Therefore, it is not possible to derive a general predictive relationship between κ_{eff} and k_s. Lower-frequency permittivity measurements (f<100 MHz), which are sensitive to surface polarization effects, can be used to predict the sample surface area, and therefore an effective pore size (e.g., Knight and Nur, 1987a; Knoll et al., 1995). However, as explained in Sections 4.5 and 4.6, it is more practical to measure these polarization effects and parameters using induced polarization methods.

In some cases, site-specific predictive relationships between κ_{eff} and k_s can be empirically developed. For example, at sites where porosity is well correlated with formation permeability, κ_{eff} can potentially be used to estimate the formation permeability (e.g., Hubbard et al., 1997). Alternatively, in partially saturated environments where the water content is often controlled by soil water-retention properties, the net water content as measured by κ_{eff} could also be a predictive measure of the formation's hydraulic properties. However, whenever possible, we recommend using κ_{eff} information in conjunction with other geophysical data such as electrical conductivity and induced polarization measurements, and advanced geostatistical interpretation tools. The site-specific empirical relationships should be based on collocated, core-scale geophysical and hydrogeologic measurements, e.g., the linear κ_{eff} ($\log(k_s)$) relationship used by Hubbard et al. (1999). These relationships, depending on their statistical significances, will probably contribute to evaluating the absolute permeabilities; if not, they will at least provide relative k_s information on an aquifer's structural heterogeneity and anisotropy at larger scales (e.g., Chen et al., 2001).

4.4 Electrical Conductivity Models

In this section, we review models for the frequency-independent conductivity response of rocks and soils. Strictly speaking, these models are applicable to low-frequency conductivity measurements where $\sigma'(\omega)$ approaches σ'_{dc} (e.g., Figure 4.1). However, because the dispersion in the conductivity response is generally much smaller than σ'_{dc}, the dispersion effects can be neglected when f < 1 MHz. The frequency

dependence in the conductivity (and permittivity) response is discussed below in Section 4.6.

The conductivity response of rocks and soils ($f < 1$ MHz) is primarily a function of the water content, the conductivity of the saturating solution, and the sample lithology. The conductivity of aqueous solutions generally increases with the concentration, mobility, and electronic charge of the ions in the solution, as well as the temperature of the solution (see Appendix). The effective shape of the grains/pores also affects the conductivity response. Surface conductivity at the grain/solution interface can also be significant in fine-grained materials, especially if the solution conductivity is low. Surface conductivity models are dependent on the amount of surface area and the surface chemical properties of the solid/liquid interface. If the solution conductivity is known, electrical conductivity measurements can be used to estimate the effective porosity of water-saturated formations or the water content of partially saturated formations. Alternatively, soil scientists often use electrical conductivity measurements to estimate soil water salinity. In some cases, electrical conductivity measurements can be used to estimate the permeability of subsurface formations. However, as described at the end of this section, these empirical correlations are quite site specific.

4.4.1 WATER-SATURATED MEDIA

Archie's empirical law (Archie, 1942) is the most widely used relationship to predict the effective electrical conductivity responses of water-saturated geological materials:

$$\sigma_{eff} = \frac{\sigma_w}{F} = \sigma_w n^m . \tag{4.26}$$

The electrical formation factor F is an intrinsic measure of material microgeometry

$$F = n^{-m}, \tag{4.27}$$

and it is often assumed to be an indicator of the hydraulic tortuosity (Equation 4.4). Archie found that the exponent m ranged from 1.3 for unconsolidated sands to approximately 2.0 for consolidated sandstones (see Table 4.1 and Figure 4.5). As m increases with cementation, Archie termed it the cementation index. Theoretically derived petrophysical models, which are discussed later in this section, relate the cementation index to the effective grain shape. Jackson et al. (1978) made electrical conductivity measurements on natural and artificial sand samples. They determined that the cementation index increased as the grains became less spherical (see Figure 4.5) while variations in grain size and sorting had little effect on m. Archie's law implicitly assumes that the effective porosity (n_e) is equal to the total porosity (n) of the sample, and that all electrical conduction in a water-saturated rock or soil results from the migration of ions in the bulk pore-solution. If there are isolated pores through which ions cannot migrate, then $n_e<n$, and Archie's law will overpredict sample conductivity.

Table 4.1. Archie's law exponents (*m*) of different consolidated and nonconsolidated media

I. MEDIUM	Porosity Range	m, Archie's Exponent	*Reference*
clean sand	0.12-0.40	1.3	Archie (1942)
consolidated sandstones	0.12-0.35	1.8-2.0	
glass spheres	0.37-0.40	1.38	Wyllie and Gregory (1955)
binary sphere mixtures	0.147-0.29	1.31	
cylinders	0.33-0.43	1.47	
disks	0.34-0.45	1.46	
cubes	0.19-0.43	1.47	
prisms	0.36-0.52	1.63	
8 marine sands	0.35-0.50	1.39-1.58	Jackson et al. (1978)
glass beads (spheres)	0.33-0.37	1.20	
quartz sand	0.32-0.44	1.43	
rounded quartz sand	0.36-0.44	1.40	
shaley sand	0.41-0.48	1.52	
shell fragments	0.62-0.72	1.85	
fused glass beads	0.02-0.38	1.50	Sen et al. (1981)
fused glass beads	0.10-0.40	1.7	Schwartz and Kimminau (1987)
sandstone	0.05-0.22	1.9-3.7	Doyen (1988)
polydisperse glass beads	0.13-0.40	1.28-1.40	de Kuijper et al. (1996)
fused glass beads	0.10-0.30	1.6-1.8	Pengra and Wong (1999)
sandstones	0.07-0.22	1.6-2.0	
limestones	0.15-0.29	1.9-2.3	
Syporex®	0.80	3.8	Revil and Cathles III (1999)
Bulgarian altered tuff	0.15-0.39*	2.4-3.3	Revil et al. (2002)
Mexican altered tuff	0.50*	4.4	
glass beads	0.38-0.40	1.35	Friedman and Robinson (2002)
quartz sand	0.40-0.44	1.45	
tuff particles	0.60-0.64	1.66	

*connected (inter-granular) porosity

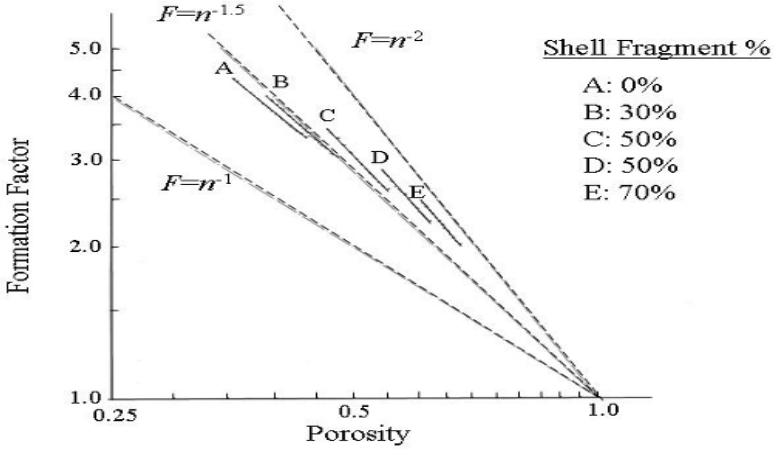

Figure 4.5. A log-log plot of formation factor versus porosity for granular mixtures consisting of rounded quartz grains and platey shell fragments (after Jackson et al., 1978, Figure 8). The dashed lines are Archie's law predictions for cementation indicies of 1.0, 1.5, and 2.0.

In fine-grained materials or in materials saturated with resistive pore solutions, surface conduction can be significant, causing Archie's law to underpredict the electrical conductivity of the sample. The conductivities of two sandstone cores measured as a function of solution conductivity are plotted in Figure 4.6 (Waxman and Smits, 1968). For the clean sandstone sample C1, the surface conductivity effects are negligible, and Archie's law is valid. The formation factor can simply be computed as the ratio of σ_w / σ_{eff}, and if the sample porosity is known, the cementation index can be computed using Equation (4.27). For the shaly sandstone sample C26, however, significant surface conductivity effects occur that result in a nonlinear relationship between σ_{eff} and σ_w. Archie's law can be modified to include a surface conduction term in parallel with the bulk conduction term, which results from the migration of ions through the bulk pore solution (e.g., Schön, 1996):

$$\sigma_{eff} = \frac{\sigma_w}{F} + \sigma_{surface} . \tag{4.28}$$

Although the bulk and surface conduction mechanisms do not strictly act in parallel (e.g., Friedman, 1998b), this simple parallel-conduction model has several practical advantages. One major advantage is that F and $\sigma_{surface}$ can be easily estimated by plotting on a linear scale σ_{eff} versus σ_w. The formation factor can be estimated from the slope of the linear portion of the σ_{eff} versus σ_w plot at high solution conductivity, and $\sigma_{surface}$ can be estimated from the extrapolated y-intercept at $\sigma_w = 0$ (e.g., Waxman and Smits, 1968; Nadler, 1982).

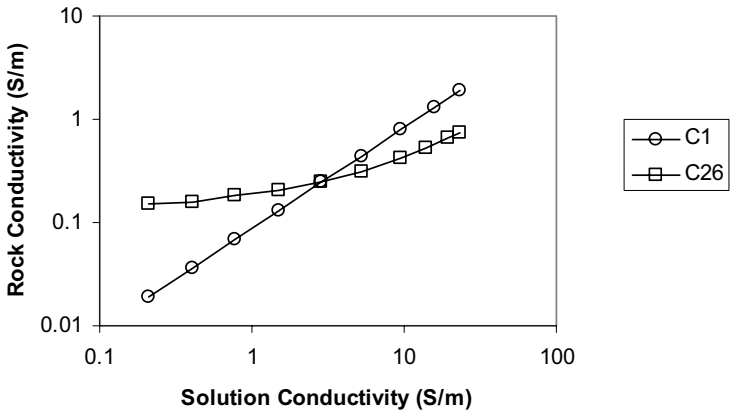

Figure 4.6. Conductivity of two sandstone cores measured as a function of the NaCl solution conductivity (Waxman and Smits, 1968). Surface conductivity effects are negligible in core C1 (n=0.239, Q_v=0.017 meq/cm^3) and significant in core C2 (n=0.229, Q_v=1.47meq/cm^3), which has a much higher cation exchange capacity.

The effects of lithology and solution chemistry on the surface conductivity term in Equation (4.28) were accounted for by Waxman and Smits (1968) in the following model:

$$\sigma_{surface} = \frac{BQ_v}{F}. \tag{4.29}$$

The cation exchange capacity per unit pore volume, Q_v, is a measure of the effective clay content, and B is the equivalent ionic conductance of the clay exchange cations. Waxman and Smits empirically obtained the following formula for the dependence of B on the solution conductivity:

$$B = \alpha\left[1 - \beta \exp\left(-\gamma\sigma_w\right)\right], \tag{4.30}$$

where the fitting parameters α, β, and γ depend upon the solution type. Sen et al. (1988) developed a modified version of the Waxman and Smits model, in which the empirical parameter B is a function of the solution conductivity (σ_w in S/m) as well as the cementation index m

$$B = \frac{1.93m}{1 + 0.7/\sigma_w}. \tag{4.31}$$

The advantage of the Sen et al. model is that it accounts for lithologic effects on the surface conductivity response; however, the empirical parameters in the equation are still dependent upon the solution type. This equation provided a good fit to conductivity measurements made on a suite of 140 shaly sandstone cores (Sen et al., 1988).

More sophisticated surface conductivity models have been developed in terms of the electrical double layer (EDL) that forms between the mineral grains and the bulk pore solution (e.g., Rink and Schopper, 1974; Johnson, et al., 1986; Schwartz et al., 1989; Revil and Glover, 1997). These models can also be represented by a bulk conduction term in parallel with a surface conduction term (Equation 4.28), where

$$\sigma_{surface} \cong \frac{\Sigma_s S_p}{f}, \tag{4.32}$$

with Σ_s the specific surface conductance, S_p the specific surface area, and f a parameter characterizing the "tortuosity" of the surface, which is similar to, but not necessarily equal to, the formation factor (e.g., Johnson, et al.; 1986). The specific surface conductance (Σ_s) represents the conduction in the fixed and diffuse parts of the electric double-layer (EDL). In general, Σ_s can be expressed as a function of the mineral surface charge density (Ω_0) and the surface ionic mobility (μ_S), such that

$$\sigma_{surface} \cong \frac{e\mu_s\Omega_0 S_p}{f}, \tag{4.33}$$

where e is the electronic charge. The charge within the EDL (Ω_0) is partitioned between the fixed layer (Ω_f) and the diffuse layer (Ω_d). The specific mobility of each ion within the EDL is a function of the ionic radius, valence, and the ion's distance from the mineral surface. Therefore, μ_S is an effective or average surface ionic mobility for the ensemble of counter-ions within the fixed and diffuse parts of the EDL (Revil

and Glover, 1997). Surface complexation models can be used to predict the surface conductivity response as a function of the geochemical parameters Ω_0 and μ_S, which vary with solution type, concentration, and mineralogy. In practical applications, however, it is usually impossible to constrain all of these parameters for a formation. Therefore, semi-empirical equations such as those developed by Waxman and Smits (1968) and Sen et al. (1988) are typically used to interpret electrical conductivity measurements of shaly sand formations or clay rich soils. For simplicity, it is assumed in Equation 4.28 that the bulk and surface conduction mechanisms are independent of each other, and that they act in parallel. Three-dimensional networks of conductors can be used to more accurately model the interactions between the bulk and surface conduction mechanisms (e.g., Bernabe and Revil, 1995; Friedman, 1998b). However, these network models are not very applicable in practical applications.

The mean field theories introduced in Section 4.3 above can also be used to model the effective conductivities of two- and three-phase mixtures. For example, the "universal" mixing formula for conductivity is obtained by replacing the relative permittivity parameters in Equation (4.19) (κ^i_{eff}, κ_w, κ_s) with the corresponding conductivity parameters (σ^i_{eff}, σ_w, σ_s). If the solid-phase conductivity is negligible, then σ_s=0 and the Maxwell-Garnet formula for electrical conductivity (a=0) is given by

$$\sigma^i_{eff} = \sigma_w \left(1 - \frac{(1-n)}{1+(1-n)N^i} \right). \tag{4.34}$$

The conductivity of an isotropic mixture of spheroids with random orientations can similarly be obtained from Equation (4.20). This model assumes that there are no interactions between the embedded particles; therefore, this Maxwell-Garnet formula results in a maximum estimate for the conductivity of a mixture, and it is most appropriate for high-porosity soils and granular materials.

The self-similar model (Equation 4.22) for the effective conductivity of a mixture of randomly oriented spheroidal grains is given by

$$\sigma_{eff} = \sigma_w n^m \left(\frac{1-\sigma_s/\sigma_w}{1-\sigma_s/\sigma_{eff}} \right)^m. \tag{4.35}$$

The self-similar model accounts for strong interactions between the embedded particles and can be used to predict the conductivity of rocks and lower porosity soils. The cementation exponent m is determined by the effective grain shape as expressed by Equation (4.23). If $\sigma_s \cong 0$, which is true for most nonmetallic minerals, the self-similar model reduces to Archie's law (Sen et al., 1981). Bussian (1983) used Equation (4.35) with a non-zero σ_s term to model the shaly sandstone conductivity measurements of Waxman and Smits (1968). In this approach, the σ_s term represents both the conductivity of the dry mineral grain (essentially zero) and the surface conduction effects. As the surface conductivity increases with increasing specific surface area (e.g., Equation 4.33), $\sigma_{surface}$ will increase with decreasing grain size. It will also be

dependent upon the surface charge density and surface ionic mobility, which vary with the solution conductivity. Although the surface conductivity mechanisms are not explicitly accounted for in Bussian's model, the interaction between the surface and bulk conduction mechanisms is treated more realistically than in the parallel conduction model (Equation 4.28). Furthermore, as is discussed in Section 4.6 below, a similar approach can be used to explicitly account for the surface conductivity mechanisms and to simultaneously predict the conductive and dielectric properties of rocks and soils.

4.4.2 UNSATURATED MEDIA

In his seminal paper, Archie (1942) also addressed the effects of saturation on the conductivity responses of consolidated and unconsolidated geological materials. Archie observed that the formation conductivity increased with saturation (S) according to the following power law:

$$\sigma_{eff}(S) = \sigma_{sat} S^{d}, \tag{4.36}$$

where σ_{sat} is the conductivity of the fully saturated sample. The saturation index d was observed to be about 2 for consolidated rocks and to range from 1.3 to 2 for unconsolidated sands (e.g., Schön, 1996). This power law was observed to hold down to saturations of about 0.15 to 0.20. At lower saturations, the power law breaks down, especially in fine-textured materials, as surface effects become dominant. In the absence of surface conductivity, the extended form of Archie's law can be used to predict the conductivity of partially saturated rocks and soils:

$$\sigma_{eff} = \sigma_w n^m S^d. \tag{4.37}$$

The saturation index is usually larger than the cementation index ($d>m$), because as saturation decreases, the water films surrounding the grains become thinner and the conducting paths become more tortuous. For coarse-textured sands, for example, the semi-empirical model of Mualem and Friedman (1991) predicts that $m=1+\gamma$ and $d=2+\gamma$, where the tortuosity exponent γ can be taken as 0.5 (Equation 4.11), making m=1.5 and d=2.5. Waxman and Smits (1968) also studied the effects of saturation on the electrical conductivity of oil-bearing shaly sandstones. They proposed the equation

$$\sigma_{eff} = \frac{S^d}{F}\left(\sigma_w + BQ_v / S\right). \tag{4.38}$$

The surface conductivity term (BQ_v/S) increases with decreasing saturation, which Waxman and Smits attributed to an increase in the volume concentration of clay exchange cations at low saturation.

Soil scientists often express the electrical conductivity in terms of water saturation (Mualem and Friedman, 1991; Weerts et al., 1999). If we assume for simplicity that $m=d$ in Archie's model, then the conductivity is given by

$$\sigma_{eff} = \sigma_w \theta^m. \tag{4.39}$$

This approach was used by Amente et al. (2000), who obtained an average exponent of m=1.58 by fitting Equation (4.39) to conductivity measurements of sandy loam soils. If

the water content is independently determined, for example by using TDR measurements of permittivity and a model such as that given by (4.25), then the soil water conductivity can be estimated using Equation (4.39), with an average m determined for the field site. The most commonly used empirical equation to predict the electrical conductivity of soils in terms of the water content is that of Rhoades et al. (1976), who assumed that the surface conductivity term ($\sigma_{surface}$) is independent of θ and σ_w:

$$\sigma_{eff} = \sigma_w \theta T_c(\theta) + \sigma_{surface}; \qquad T_c(\theta) = a\theta + b. \tag{4.40}$$

The transmission coefficient $T_c(\theta)$ is assumed to be a linear function of θ, and the empirical coefficients a and b are a function of the soil type. For clay soils, a=2.1 and b=-0.25; for loam soils, $1.3 \le a \le 1.4$ and $-0.11 \le b \le -0.06$ (Rhoades et al., 1976).

Effective media theories and network models can also be used to model the effects of partial saturation on the electrical conductivity responses of rocks and soils (e.g., Feng and Sen, 1985; Man and Jing, 2001). These models can be used to better understand the various structural factors controlling the conductivity responses of rocks and soils, and to investigate important phenomena such as hysteresis. In practical applications, however, there is usually never enough information to constrain all of the parameters in the theoretically based models. Therefore, more empirically based approaches are typically used to interpret field measurements.

4.4.3 PERMEABILITY ESTIMATION

The Kozeny-Carman (K-C) permeability model (Equation 4.3) forms the basis of many permeability prediction equations (e.g., Nelson, 1994). In Equation (4.5), obtained from the K-C model, the formation factor (F) and the specific surface area (S_p) are the two key parameters needed to predict permeability. Because the formation factor can be estimated from electrical conductivity measurements, it is not surprising that many investigators have tried to use this approach for *in situ* permeability estimation (e.g., Nelson, 1994). In fact, in his seminal paper, Archie (1942) showed good correlations between k_s and $1/F$ for his suite of consolidated sandstone cores. Anisotropy measurements for the electrical conductivity of cores can also be used to estimate anisotropy in the permeability of the samples (Friedman and Jones, 2001). These approaches are limited, however, because S_p, which is a measure of the effective pore size, is much more variable than F for rock and soil formations. Therefore, in practice, F is of secondary importance in predicting the permeability of rock and soil formations. Electrical estimation of the effective pore/grain size using induced polarization methods is the focus of Sections 4.5 and 4.6 below.

Several empirically based equations have been proposed to electrically predict the permeability (or hydraulic conductivity) of rock and soil formations (e.g., Heigold et al., 1979; Huntley, 1986; Kosinski and Kelly, 1981; and Purvance and Andricevic, 2000). These equations, which are site specific, can be categorized into two groups. For clay-free formations and coarse-textured soils, the permeability and conductivity tend to be positively correlated, because they both increase with increasing porosity (or decreasing F), as is predicted by the K-C model (e.g., Heigold et al., 1979). For shaly

sand formations and fine-textured soils, where surface conductivity effects are significant, the permeability and electrical conductivity tend to be inversely correlated (e.g., Kosinski and Kelly, 1981). Increasing clay content causes the permeability to decrease as the effective size of the pores is decreased, but it causes the electrical conductivity to increase because of increasing surface conductivity effects. This inverse correlation between k_s and σ_{eff} is often enhanced in partially saturated formations, where high-permeability materials tend to drain faster and have lower water-retention properties (i.e., lower field capacity) than low-permeability materials. Since the electrical conductivity is also a function of water content, high permeability soils tend to be drier and have lower conductivities than lower permeability soils.

4.5 Induced Polarization Models

Historically, IP methods have been used mostly to explore for metallic ore deposits. Recently, however, they are increasingly being used in a wide variety of environmental and engineering applications (e.g., Slater and Lesmes, 2002a; Chapter 5 of this volume). The IP response of non-metal-bearing earth materials is primarily controlled by the effective clay content or internal surface area of the sample (e.g., Vinegar and Waxman, 1984; Börner and Schön, 1991). Because the permeability of rocks and soils is also strongly dependent upon these "lithologic" parameters it is possible to develop permeability prediction equations in terms of the measured IP response of the sample (e.g., Börner et al., 1996; Slater and Lesmes, 2002b). The effectiveness of IP-permeability prediction formulae is complicated by the dependence of the IP response on secondary factors, such as the type of clay and its distribution, the solution conductivity and composition, the organic matter content, and water saturation. Because of these complicating factors, IP-permeability prediction formulae must be calibrated for the conditions at specific sites. However, the IP-permeability predictions are generally more accurate and robust than those made using high-frequency permittivity measurements or low-frequency conductivity measurements, as discussed in Sections 4.3 and 4.4 above. The IP (or complex conductivity) response is also a function of frequency; but over the frequency range of typical field instruments (10^{-2} Hz to 10^{2} Hz) the IP responses of many earth materials are relatively constant. In this section, we review models for the frequency-independent IP parameters typically measured in the field. In the next section, we review more comprehensive models for the broadband complex-conductivity responses of rocks and soils as measured in the laboratory. In the remainder of this chapter, we will refer to the effective complex conductivity σ^*_{eff} as simply σ^* and to the effective complex permittivity as ε^*_{eff} as ε^*. The relationship between these complex electrical parameters is defined by Equation (4.12).

4.5.1 INDUCED POLARIZATION PARAMETERS

Field IP surveys can be conducted using complex resistivity (CR), frequency-domain IP, or time-domain IP measurement systems (e.g., Ward, 1990). All of these systems are operationally similar to the DC resistivity method. However, in addition to

measuring the conductive properties of the media, IP systems also measure, either directly or indirectly, the low-frequency capacitive properties of the media. The proportionality between the CR phase (θ), percent frequency effect (PFE), and chargeability (M) is both theoretically and experimentally well established (e.g., Marshall and Madden, 1959; Vinegar and Waxman, 1984). These field IP parameters, defined in Table 4.2, effectively measure the ratio of the capacitive to conductive properties of the material at low frequencies. The low-frequency capacitive component (σ'') is primarily controlled by electrochemical polarization mechanisms, whereas the low-frequency conductive component (σ') is primarily controlled by electrolytic conduction in the bulk pore solution and can be modeled using all the relationships presented in the previous section. Therefore, the field IP parameters are sensitive to the ratio of surface conductivity to bulk conductivity effects (e.g., Lesmes and Frye, 2001; Slater and Lesmes, 2002a).

Dividing the field IP parameters by the formation resistivity, or multiplication by the formation conductivity, yields the following normalized IP parameters: quadrature conductivity or imaginary conductivity (σ''), metal factor (MF), and a normalized chargeability (MN). These normalized IP parameters, defined in Table 4.2, are more directly related to the surface chemical properties of the material. Normalized IP parameters are therefore useful for characterizing lithological and geochemical variability (e.g., Lesmes and Frye, 2001; Slater and Lesmes, 2002a). In the rest of this section, the IP data and models are expressed in terms of the real and imaginary components of the complex conductivity, where the imaginary conductivity is directly proportional to the other normalized IP parameters, MN and MF.

Table 4.2. Commonly measured field IP parameters (θ, PFE*, and M) are equivalent measures of the IP response. The normalized IP parameters (σ'', MF, and MN) are more directly related to the surface properties of the rock/soil sample.*

Field IP Parameters	**Normalized IP Parameters**
$\theta = \tan^{-1}\left(\sigma'' / \sigma'\right) \cong \sigma'' / \sigma.'$	$\sigma'' = \sigma' \tan(\theta) \cong \sigma'\theta$
$PFE = 100 * \dfrac{\sigma(\omega_1) - \sigma(\omega_0)}{\sigma(\omega_0)}.$	$MF = a\left(\sigma(\omega_1) - \sigma(\omega_0)\right)$
$M = \dfrac{1}{V_{\max}(t_1 - t_0)} \int_{t_0}^{t_1} V(t)dt.$	$MN = M\sigma'$

*PFE is the relative dispersion in the conductivity response measured between a low frequency (ω_0) and a higher frequency (ω_1); a is a dimensionless constant; $V(t)$ is the potential difference measured at a time t after the current is shut off, V_{max} is the maximum potential difference measured during current transmission, and t_0 and t_1 define the time window over which the voltage decay curve is integrated.

4.5.2 WATER-SATURATED MEDIA

In a classic study, Vinegar and Waxman (1984) measured the complex conductivity response of a suite of 21 shaly sandstone cores as a function of pore water conductivity. They used this data set to develop the following complex form of the Waxman and Smits (1968) surface conductivity model

$$\sigma^* = \frac{1}{F}\left(\sigma_w + BQ_v\right) + i\frac{\lambda Q_v}{Fn}. \tag{4.41}$$

The real part of Equation (4.41) is Waxman and Smits (1968) model, in which the bulk and surface conduction terms are assumed to add in parallel. The imaginary (or quadrature) conductivity results from displacement currents that are 90 degrees out-of-phase with the applied field. Vinegar and Waxman assumed that the displacement currents were caused by the following two polarization mechanisms: (1) the blockage of ions by clay minerals at pore throats (membrane polarization) and (2) the accumulation of counter-ions migrating along grain/pore surfaces. Although these polarization mechanisms are intrinsically frequency dependent, Vinegar and Waxman showed that over the low frequency range of their measurements (3 Hz to 1 kHz), the quadrature conductivity response was essentially independent of frequency. Vinegar and Waxman assumed that both the membrane and the counter-ion polarization mechanisms were proportional to the effective clay content or specific surface area, represented by the cation exchange capacity of the rock per unit pore volume (Q_v). The parameter λ in Equation (4.41) represents an effective quadrature conductance for these surface polarization mechanisms, and it is analogous to the specific surface conductance term (Σ_s) in Equation (4.32). Vinegar and Waxman empirically determined λ to be slightly dependent on salinity. The polarization was also assumed to increase with decreasing porosity, as more pores become blocked.

4.5.3 UNSATURATED MEDIA

Vinegar and Waxman also measured the complex conductivity responses of their samples as a function of the water/oil saturation. Following the approach of Waxman and Smits (1968), they assumed that the effective cation exchange capacity would increase with decreasing saturation, such that $Q_v^{'} = Q_v / S$. The imaginary conductivity therefore had the following dependence upon saturation: $\sigma^{"}(S) = \sigma_{sat}^{"} S^q$, where $\sigma_{sat}^{"}$ is the imaginary conductivity of the fully saturated sample. They observed that $q \cong d - 1$ where d is the saturation index for the real conductivity (Equation 4.36). Their measurements confirmed the validity of this expression for their samples. Ulrich and Slater (2004) measured the complex conductivity responses of unconsolidated sediments as a function of the water/air saturation. They observed a similar power-law dependence of the imaginary conductivity on water saturation, with the saturation exponent of the imaginary conductivity being less than the saturation index for the real conductivity ($q<d$). They also observed that the imaginary conductivity was a function of the saturation history (i.e., hysteretic effects). Effective media theories, discussed in

more detail in Section 4.6 below, can be used to model the effects of saturation on the complex conductivity response (e.g., Endres and Knight, 1992; Samstag, 1992).

4.5.4 PERMEABILITY ESTIMATION

Börner and Schön (1991) established the following linear relationship between S_p and σ'', based on complex conductivity measurements made on unconsolidated sediments at a frequency of 1 Hz (see Figure 4.7):

$$S_{p[el]} = b(\sigma''_{1Hz}), \tag{4.42}$$

where $S_{p[el]}$ is in μm^{-1}, σ''_{1Hz} is in S/m, and $b = 10^{-11}\,S^{-1}$. Using this relationship in a KC-type model, they obtained the following expression for the hydraulic conductivity:

$$K_s = \frac{a}{FS^c_{p[el]}} = \frac{a}{F\left(10^5\,\sigma''_{1Hz}\right)^c} \tag{4.43}$$

where K_s is in m/s, a=10^{-5} and c ranged between 2.8 and 4.6, depending upon the material type and the method used to measure K_s.

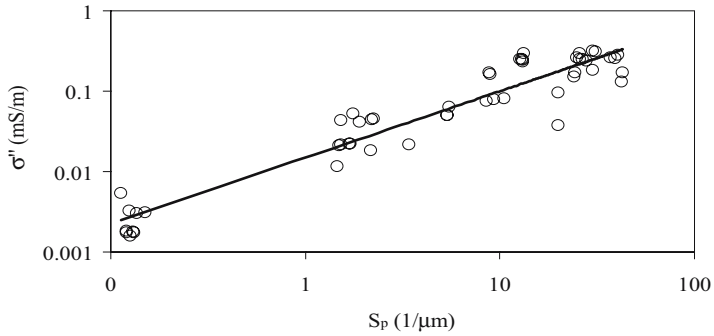

Figure 4.7. Börner and Schön (1991) observed a linear correlation between the imaginary conductivity of their saturated sandstone samples and the specific surface area. The samples were saturated with 0.01 M NaCl and measured at a frequency of 1 Hz.

Slater and Lesmes (2002b) measured the complex conductivity response and hydraulic properties of sand-clay mixtures and glacial tills. They observed a power law relationship between S_p and σ''_{1Hz}:

$$S_{p[el]} = 2000\left(\sigma''_{1Hz}\right)^p, \tag{4.44}$$

where p=0.5±0.2 (R^2=0.53, CI=95%). This relationship also appeared to be a function of the material type. They found for their samples, however, that σ'' was better correlated with the effective grain size d_{10} (see Figure 4.8):

$$\sigma''_{1Hz} = 0.0005\left(d_{10}\right)^{-b}, \tag{4.45}$$

where d_{10} is in μm, σ'' is in S/m, and b=1.0±0.1 (R^2=0.83, CI=95%). Using a Hazen type of grain permeability model (Equation 4.6), they obtained the following expression for the hydraulic conductivity in terms of σ'':

$$K_s = a\left(\sigma''_{1Hz}\right)^b, \tag{4.46}$$

where a=800±1200 and b=1.1±0.2 (σ'' is in S/m, K_s in m/s, R^2=0.7).

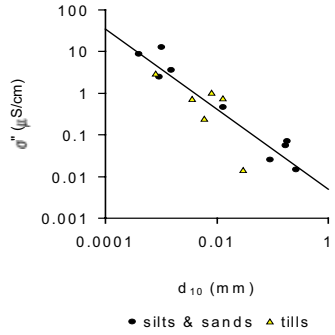

Figure 4.8. Imaginary conductivity of unconsolidated sand samples plotted as a function of the effective grain size d_{10} (Slater and Lesmes, 2002b). The complex conductivity was measured at 1 Hz, and the samples were saturated with 0.01 M NaCl.

A cross plot of the predicted-versus-measured hydraulic conductivity measurements is shown in Figure 4.9. The samples indicated by the + symbol in Figure 4.9 were not part of the data set used to establish the relationship between σ''and d_{10} in Equation (4.45), so they serve as an independent check on the robustness of this predictive equation.

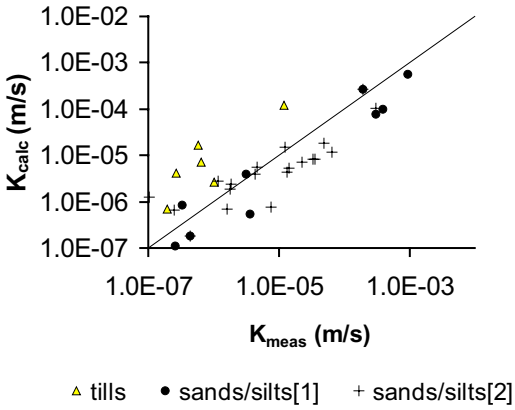

Figure 4.9. Cross plot of the predicted and measured hydraulic conductivity of the unconsolidated samples plotted in Figure 4.8. The hydraulic conductivity was predicted from the measured imaginary conductivity using Equation (4.46). The samples indicated by the + symbol were not used to establish the relationship in Equation (4.46), and they therefore are an independent check on the robustness of this permeability predication equation (Slater and Lesmes, 2000b).

The model consistently overpredicts the K_s values for the glacial till samples, indicated by the triangles in Figure 4.9. These samples are highly heterogeneous and have broad grain-size distributions. More accurate permeability predictions could perhaps be achieved by taking into account additional factors such as the grain sorting. As is discussed in Section 4.6, this additional information may possibly be obtained by measuring the frequency dependence in the imaginary conductivity response.

The development of permeability prediction equations using normalized IP parameters such as σ'' seems promising. However, the normalized IP parameters can also vary with solution chemistry, which can complicate the predictive relationships between the IP parameters and the desired lithologic variables. For example, the imaginary conductivity response of three shaly sandstone samples measured by Vinegar and Waxman (1984) are plotted versus solution conductivity in Figure 4.10. This plot shows that σ'' increases with increasing clay content, as expected, but there is a non-monotonic dependence upon solution conductivity, which increases with increasing clay content. Using a more sophisticated shaly sand model, de Lima and Niwas (2000) were able to account for the salinity dependence of σ'' and obtained a good prediction of the permeabilities of the Vinegar and Waxman samples. However, the model was significantly more complicated than, for example, Equation (4.46), and it would be difficult to constrain all of the model parameters without having complex conductivity measurements of the core samples made as a function of salinity. Therefore, this approach is difficult to apply in the practical interpretation of field data sets.

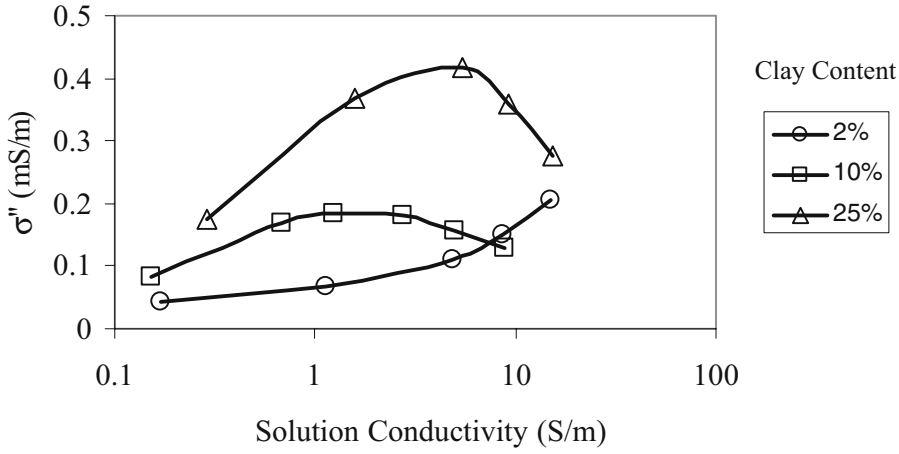

Figure 4.10. Imaginary conductivity of shaly sandstone samples plotted as a function of the solution conductivity (Vinegar and Waxman, 1984). Although the imaginary conductivity generally increases with increasing clay content, it has a nonmonotonic dependence upon the solution conductivity.

4.6 Complex Conductivity Models

The dispersion in the conductivity and dielectric responses of rocks and soils is controlled by physical and chemical polarization mechanisms that result in a broad distribution of relaxation times. To characterize the electrical properties of a sample fully requires that the impedance response be measured over a very wide range of frequencies (e.g., 10^{-3} Hz to 10^{9} Hz), so that the entire distribution of relaxation times can be captured (e.g., Olhoeft, 1985, 1986; Lesmes and Morgan, 2001). To span this frequency range requires using three different measurement systems with different sample configurations, which is both costly and time consuming. In most laboratory investigations, a single type of measurement system is used to characterize the impedance response over a limited range of frequencies while varying the sample lithology, solution chemistry, and water saturation. These data can be used to partially test models for the frequency-dependent complex conductivity responses of rocks and soils, but broadband data, collected from the low- to high- frequency limits, are required to fully constrain all of the model parameters. In this section, we review both empirical and theoretical models for the broadband complex conductivity responses of rocks and soils, and try to establish connections between the empirical and theoretical model parameters. We also discuss how broadband complex conductivity measurements and models can perhaps be used to more accurately predict the hydraulic properties of rocks and soils in the laboratory and in the field.

4.6.1 EMPIRICAL MODELS

Relatively simple empirical models can be used to fit the frequency-dependent permittivity and conductivity responses of rocks and soils. Havriliak and Negami (1967) introduced the following empirical dielectric response function, which is a generalized form of the widely used Cole-Cole (1941) and Cole-Davidson (1950) dielectric models:

$$\varepsilon^*_{HN}(\omega) = \frac{\Delta\varepsilon}{(1+(i\omega\tau_o)^{1-\alpha})^{\beta}}. \tag{4.47}$$

Equation (4.47) only predicts the frequency dependence in the permittivity and conductivity responses. It does not account for the high-frequency permittivity response (ε_∞) or the low-frequency conductivity response (σ_{dc}) of the sample. Specific models for ε_∞ and σ_{dc} were discussed above in Sections 4.3 and 4.4, respectively. One approach to modeling the "complete" response (the frequency-dependent and independent properties of a sample) is to assume that the ε_∞ and σ_{dc} terms act in parallel with the dispersive term $\varepsilon^*_{HN}(\omega)$ in Equation (4.47), such that the "complete" complex permittivity response is given by:

$$\varepsilon^*(\omega) = \left(\varepsilon_\infty + \frac{\sigma_{dc}}{i\omega}\right) + \frac{\Delta\varepsilon}{(1+(i\omega\tau_o)^{1-\alpha})^{\beta}}. \tag{4.48}$$

The Havriliak-Negami (HN) equation simplifies to the Cole-Cole (CC) expression when $\beta = 1$, it reduces to the Cole-Davidson (CD) expression when $\alpha = 0$, and it

simplifies to the Debye expression when $\alpha = 0$ and $\beta = 1$. The dielectric increment $\Delta\varepsilon=\varepsilon_{static}-\varepsilon_{\infty}$ determines the amount of dispersion in the dielectric and conductivity responses, the central relaxation time τ_0 determines the characteristic angular frequency ($\omega_0 = 2\pi f_0 = 1/\tau_0$) of the relaxation, and the exponents α and β determine the shape of the relaxation (e.g., Bottcher and Bordewijk, 1978). To accurately estimate the model parameters, the dielectric response must be measured from the low- to high-frequency limits. These broadband measurements are difficult to make in the laboratory and essentially impossible to make in the field. Therefore, models such as the Cole-Cole response are often not fully constrained by the available data, and the model parameters obtained by inversion are non-unique.

If the relaxation in the permittivity and conductivity responses cannot be fully captured, then it is better to use models with fewer parameters to more uniquely fit the available data. For this reason, the constant phase-angle (CPA) model is widely used to model the dispersion in the complex conductivity responses of rocks and soils:

$$\sigma^*_{CPA}(\omega) = \sigma_0 (i\omega/\omega_0)^p = \sigma_0 (\omega/\omega_0)^p e^{ip\pi/2}. \tag{4.49}$$

In the CPA model, σ_0 is the magnitude of the complex conductivity response measured at an arbitrary angular frequency of ω_0. The dispersion parameter p determines both the phase angle $\theta = p\pi/2$ and the rate of change for the conductivity amplitude with increasing frequency. Adding the frequency-independent terms ε_{∞} and σ_{dc} in parallel with the dispersive CPA response gives:

$$\sigma^*(\omega) = (\sigma_{dc} + i\omega\varepsilon_{\infty}) + \sigma_0 (\omega/\omega_0)^p e^{ip\pi/2}. \tag{4.50}$$

To fit Equation (4.50) to complex conductivity measurements, the reference frequency ω_0 must be arbitrarily defined (e.g., f_0=1Hz or $\omega_0 = 2\pi$ radians/sec). Furthermore, unless very broadband data are used, the estimates of σ_{dc} and ε_{∞} will change with the frequency range of the measurement, such that: $\sigma_{dc} \cong \sigma'(\omega_{\min})$ and $\varepsilon_{\infty} \cong \varepsilon'(\omega_{\max})$. Although these parameters are not uniquely defined, it is important to include them in the inversion to obtain a good fit to the data and to accurately estimate σ_0 and p.

It is instructive to compare the CPA model to the high-frequency limit $(\omega >> 1/\tau_0)$ of the Cole-Cole model, for which the complex conductivity response is given by

$$\sigma^*_{CC}(\omega) \cong \frac{\Delta\varepsilon}{\tau_0}(i\omega\tau_0)^{\alpha} = \frac{\Delta\varepsilon}{\tau_0}(\omega\tau_0)^{\alpha} e^{i\alpha\pi/2}. \tag{4.51}$$

The relationships between the CPA and Cole-Cole model parameters is as follows: $\sigma_0 = \Delta\varepsilon/\tau_0$, $\omega_0 = 1/\tau_0$, and $p = \alpha$. This comparison illustrates the utility of the CPA model when fitting narrow band data. In the rest of this chapter, we use theoretically based models and published data to try to establish the physical and chemical significance of the empirical model parameters from the Cole-Cole and CPA models.

4.6.2 THEORETICAL MODELS

Theoretically based effective medium theories can be used to simultaneously model the conductivity and permittivity responses of rocks and soils. The Bruggeman-Hanai-Sen (BHS) effective medium model (Bruggeman, 1935; Hanai, 1960; Sen et al., 1981) is a complex form of the self-similar, asymmetric, effective media theories used to model the high-frequency permittivity (Equation 4.22) and the low-frequency conductivity (Equation 4.35) responses of rocks and soils:

$$\varepsilon^* = \varepsilon_w^* n^m \left(\frac{1 - \varepsilon_s^* / \varepsilon_w^*}{1 - \varepsilon_s^* / \varepsilon^*} \right)^m . \tag{4.52}$$

The cementation index m is a function of the grain shape, and for isotropic mixtures it is defined by Equation (4.23). The complex permittivity of the pore water is a function of frequency:

$$\varepsilon_w^* = \varepsilon_0 \kappa_w + i\omega\sigma_w . \tag{4.53}$$

If surface conductivity and polarization effects are neglected, then the complex permittivity of the mineral grains is purely real and frequency independent: $\varepsilon_s^* = \varepsilon_s'$. The conductivity and permittivity responses predicted by the BHS model have relaxations at relatively high frequencies (MHz range), and the relaxation frequency increases with increasing solution conductivity (e.g., Kenyon, 1984). The magnitude of the dispersions in the permittivity and conductivity responses increases slightly with increasing m, but the predicted dispersions are much smaller than observed permittivity and conductivity responses of rocks and soils (e.g., Lesmes and Morgan, 2001).

The BHS model represents the bulk properties of the rock/soil system. However, the surface phase that forms between the mineral grains and the pore solution can significantly affect both the conductive and capacitive properties of rocks and soils. Excess conduction and polarization at the solid/liquid interface leads to enhanced conductivity and permittivity responses that are frequency dependent. When ions migrate through water-bearing rocks and soils, they can accumulate at pore throat constrictions, at blockages caused by clay minerals, or on rough grain/pore surfaces. The re-equilibration of these charge accumulations is a diffusion-controlled process. Therefore, the time that it takes the charges to re-equilibrate is dependent upon the distances over which they are polarized. Complex conductivity measurements (such as those for Berea sandstone shown in Figure 4.1) can be inverted for a distribution of diffusive relaxation times, which can be transformed into a distribution of diffusion lengths. The diffusion-length distribution can then be equated to an effective distribution of grain or pore sizes, depending upon the specific geometries used to model the diffusive polarization mechanisms (e.g., Morgan and Lesmes, 1994; Chelidze and Guegen, 1999; Chelidze et al, 1999; Lesmes and Morgan, 2001).

Theoretical models have been derived for a variety of diffusive polarization mechanisms that can contribute to the permittivity and conductivity responses of water-bearing rocks and soils (Marshall and Madden, 1959; Schwarz, 1962; Wong,

1979; Chew and Sen, 1982, de Lima and Sharma, 1992). All of these models are similar in that the relaxation time distribution, which controls the dispersions in the conductivity and permittivity responses, is determined by the distribution of diffusion lengths. The characteristic lengths in the models can be grain size, pore size, the spacing between clay blockages of pore throats, or surface roughness. For simplicity, we consider just the EDL polarization model of Schwarz (1962) for a fixed-layer of charge surrounding a spherical grain. In this model, the "fixed" charge in the EDL (Ω_f) is allowed to migrate tangentially to the grain surface, but is restricted from migrating radially away from the grain. This model results in a single Debye response, where the relaxation time is a function of the particle radius (*R*) and the surface ionic mobility (μ_S) (or the surface diffusion coefficient: $D_s = \mu_s kT$):

$$\tau_0 = \frac{R^2}{2\mu_s kT}, \tag{4.54}$$

where *k* is Boltzman's constant and *T* is absolute temperature. The dielectric increment is given by

$$\Delta\varepsilon = \frac{eR\Omega_f}{kT}. \tag{4.55}$$

The polarization of a grain-size distribution, which can represent the water-wet rock matrix, will result in a distribution of relaxation times. If we use the Cole-Cole model to represent the complex permittivity response of the water-wet rock matrix (ε_m^*), then the Cole-Cole parameters can be defined in terms of the microgeometrical and surface chemical properties of the granular mixture (Lesmes et al., 2000). In this case, the central relaxation time τ_0 is approximately proportional to the grain radius (R_0) corresponding to the peak in the grain volume distribution:

$$\tau_0 \cong \frac{R_0^2}{2\mu_s kT}. \tag{4.56}$$

The dispersion parameter α is related to the width of the grain-size distribution. For fractal grain-size distributions, α can be related to the fractal dimension (*d*) of the grain-size distribution (e.g., Lesmes et al., 2000; Lesmes and Morgan, 2001):

$$\alpha \cong \frac{d-2}{2}. \tag{4.57}$$

The conductivity increment ($\Delta\sigma = \sigma_0 = \Delta\varepsilon / \tau_0$) is given by:

$$\Delta\sigma \cong \frac{e\mu_f \Omega_f S_p}{f}, \tag{4.58}$$

where f=3/2; and the dielectric increment is given by

$$\Delta\varepsilon \cong \frac{e\Omega_f S_p R_0^2}{3kT}. \tag{4.59}$$

The total response of the water-wet rock matrix will be the combination of all of the polarization mechanisms (e.g., fixed layer polarization, diffuse layer polarization, membrane polarization, etc.) and their interactions. The details of the physical and chemical interactions in the polarization models may be very complex, but laboratory experiments indicate that the net response of all of these interactions will result in a distribution of relaxation times that has a rather simple Cole-Cole type of response.

The complex electrical response of the complete sample is obtained by incorporating the response of the water-wet rock matrix into an effective media model for the entire rock or soil sample (Knight and Endres, 1990; Samstag, 1992; de Lima and Sharma, 1992). In terms of the BHS model, the complex permittivity response is given by

$$\varepsilon^* = \varepsilon_w^* n^m \left(\frac{1 - \varepsilon_m^* / \varepsilon_w^*}{1 - \varepsilon_m^* / \varepsilon^*} \right)^m , \tag{4.60}$$

and the complex conductivity response is given by

$$\sigma^* = \sigma_w^* n^m \left(\frac{1 - \sigma_m^* / \sigma_w^*}{1 - \sigma_m^* / \sigma^*} \right)^m . \tag{4.61}$$

The model for ε_m^* (or σ_m^*) will depend upon the specific polarization mechanisms that are assumed to control the complex electrical response of the water-wet rock matrix. If we assume for simplicity that ε_m^* results from fixed-layer polarization of the EDL as described above, then

$$\varepsilon_m^* = \frac{\Delta\varepsilon}{1 + (i\omega\tau_0)^{1-\alpha}} , \tag{4.62}$$

where τ_0, α, and $\Delta\varepsilon$ are given by Equations (4.56), (4.57), and (4.59), respectively. Equation (4.62) accounts for the frequency dependence in the EDL polarization as described by the Schwartz model. This model assumes that no interaction occurs between the grains, and therefore counterions in the EDL cannot migrate across multiple grain lengths. Therefore, the conductivity of the surface phase is predicted to go to zero in the low-frequency limit of Equation (4.62). To account for surface conductivity effects, Lesmes and Morgan (2001) added a surface conductivity term to the EDL polarization response. Since $\Delta\sigma$ in Equation (4.58) has the same functional form as $\sigma_{surface}$ in Equation (4.32), we can use $\Delta\sigma$ to represent the surface conductivity. The complex permittivity response of the water-wet matrix is then given by

$$\varepsilon_m^* = \frac{\Delta\varepsilon}{1 + (i\omega\tau_0)^{1-\alpha}} + \frac{\Delta\varepsilon / \tau_0}{i\omega} , \tag{4.63}$$

where $\Delta\sigma = \Delta\varepsilon / \tau_0$. This model can also be expressed as a complex conductivity and written in term of $\Delta\sigma$:

$$\sigma_m^* = \frac{i\omega\tau_0\Delta\sigma}{1+(i\omega\tau_0)^{1-\alpha}} + \Delta\sigma \,. \tag{4.64}$$

This model can be used to invert complex permittivity data for an effective grain-size distribution (Lesmes et al., 2000; Lesmes and Morgan, 2001). If the porosity, cementation index, and solution conductivity are known then Equation (4.60) can be explicitly solved for the complex permittivity of the water-wet rock matrix. Equation (4.63) can then be fit to $\varepsilon_m^*(\omega)$ in order to estimate the Cole-Cole model parameters, which can in turn be used to estimate the effective grain-size distribution of the sample (Lesmes and Morgan, 2001). For samples with significant surface polarization effects, the measured response of the sample $\varepsilon^*(\omega)$ is dominated by $\varepsilon_m^*(\omega)$, especially at lower frequencies (f<1 MHz). Therefore, fits of the Cole-Cole model to $\varepsilon^*(\omega)$ and $\varepsilon_m^*(\omega)$ will yield essentially the same estimates for τ_0 and α (Lesmes and Morgan, 2001). This may not be true, however, at higher frequencies, where the interfacial polarization mechanisms can be comparable to or greater than the electrochemical polarization mechanisms.

4.6.3 WATER-SATURATED MEDIA

In this section, we briefly review published experimental studies on the complex electrical properties of rocks and soils to illustrate how the Cole-Cole parameters τ_0 and α depend upon the sample lithology and pore solution chemistry. (For a more complete review of experimental studies, refer to Chelidze et al., 1999; and Schön, 1996.) Diffusive polarization models predict that $\tau_0 \propto R_0^2$. Complex conductivity measurements of samples with metallic grains are generally observed to follow this trend (e.g., Olhoeft, 1985); however, Pelton et al. (1978) showed that τ_0 was also a function of the particle concentration. Titov et al. (2002) measured the differential polarizability (a form of spectral induced polarization) of sieved sand samples saturated with tap water. They observed $\tau_0 \propto R_0^{1.7}$, where R_0 is the radius of the sand grains. They interpreted their results using a short-narrow-pore model, which is similar to the membrane polarization mechanism of Marshall and Madden (1959). Scott and Barker (2003) measured the complex impedance response (10^{-3} Hz to 10^3 Hz) of 18 sandstone cores and showed that there was a good correlation between the peak in the phase spectrum, which is often taken to be a measure of τ_0, and the characteristic size of the pore-throats determined by mercury injection measurements. Their data indicate that the relaxation frequency ($\omega_0 = 1/\tau_0$) varied by five orders of magnitude for approximately one order of magnitude change in characteristic pore size. This would roughly correspond to a power-law relationship of $\tau_0 \propto R_0^5$. They did not, however, provide a physical or chemical model to explain this interesting observation.

Klein and Sill (1982) measured the electrical-impedance response (10^{-3} Hz to 10^3 Hz) of glass-bead and clay mixtures, with varying pore solution chemistries. They used a form of the Cole-Cole model to invert their data for a central relaxation time and a

chargeability parameter. They showed that the relaxation time generally increased with the size of the glass beads: $\tau_0 \propto R_0^a$ where $0.5 \le a \le 1.1$. The power law exponent a was less than 2 and dependent upon the solution conductivity and the amount of clay in the mixture. These experiments indicate that the simple model in Equation (4.56) may work relatively well for a mixture of single-sized particles (e.g., Titov et al., 2002), but it seems to break down for more complicated sand-clay mixtures and lithified rocks. One of the biggest limitations of the model expressed by Equation (4.56) is that it does not take into account the interactions between the grains; it simply assumes that all of the grain polarizations are superimposed (Lesmes and Morgan, 2001).

In the Cole-Cole model, the dispersion parameter α determines the width of the relaxation time distribution (e.g., Bottcher and Bordewijk, 1978). Several investigators have derived relationships between α and the fractal dimension d (e.g., Ruffet et al., 1991). Nearly all of these models are similar to Equation (4.57) in that they predict α to increase with increasing d. Dielectric measurements of sandstone cores by Ruffet et al. (1991) and Knight and Nur (1987a) showed α to increase with the specific surface area of the sample, which is consistent with the idea that α is related to the surface roughness or fractal dimension. Glover et al. (1994) measured the dielectric response of Berea and Darley Dale sandstone cores as a function of the solution conductivity. They showed in their study that α increases with increasing solution conductivity, which is not explicitly predicted by the fractal models. One possible explanation for this observation is that the effective surface roughness increases as the EDL compresses with increasing solution concentration. This may imply that the diffuse part of the EDL is indeed contributing to the net electrochemical polarization response.

4.6.4 UNSATURATED MEDIA

Three-phase effective medium models can be used to predict the conductivity and permittivity responses of partially saturated samples (Feng and Sen, 1985; Endres and Knight, 1992; Samstag, 1992). The BHS model can be used to simulate the effects of partial saturation (e.g., water and air mixtures) by replacing ε_w^* in Equation (4.53) with the effective complex permittivity response of the water/air mixture. In this case, the BHS equation can be used to first compute the complex permittivity of the water/air mixture. Then, a second embedding is performed to mix the water-wet mineral grains into the water/air background (e.g., Samstag, 1992). In this double-embedding procedure, it is assumed that the response of the surface phase ε_m^* does not change with saturation. Knight and Nur (1987a) demonstrated that this is generally true as long as the saturation is greater than the critical saturation, which roughly corresponds to one monolayer coverage of water molecules on the pore/grain surface. They also showed that the critical saturation increased linearly with the internal surface area of the sample, and that the dispersion parameter α is relatively independent of saturation for saturations greater than the critical saturation. Below the critical saturation, the permittivity response and the dispersion parameter α rapidly decrease. The permittivity and conductivity responses are also dependent upon the saturation history: the permittivity and conductivity responses measured during imbibition are

consistently greater than the responses measured during drainage (Knight and Nur, 1987b; Knight, 1991; Roberts and Lin, 1997). Roberts and Lin (1997) showed that the hysteretic effects increased with the surface area of the sample and the solution resistivity (i.e., increasing thickness of the EDL), indicating that these effects are at least partially affected by the surface properties of the sample.

4.6.5 PERMEABILITY PREDICTION

Petrophysical models predict the permeability of rocks and soils to be proportional to the square of a characteristic pore or grain size (Friedman and Seaton, 1998): $k \propto R_0^2$ (e.g., Equations 4.3 and 4.5). Diffusion polarization mechanisms for the complex conductivity response predict that $\tau_0 \propto R_0^2$ (e.g., Olhoeft, 1985; Chelidze and Gueguen, 1999). The K-C equation (4.3) can then be expressed in terms of the electrical parameters τ_0 and F, such that (e.g., Kemna, 2000)

$$k \propto \frac{\tau_0}{F} \tag{4.65}$$

Complex conductivity or spectral IP measurements (made in the time or frequency domains) can be used to estimate τ_0 if there is sufficient bandwidth (e.g., Pelton et al., 1978; Johnson, 1984). If the pore solution conductivity is known, then the formation factor (F) can be estimated from the measured formation conductivity. Furthermore, the dispersion parameter α can be related to the width of the pore or grain-size distribution. As the permeability increases with increased sorting (e.g., Nelson, 1994), Equation (4.65) can be modified to include α as a sorting parameter (e.g., Kemna, 2000):

$$k \propto \frac{\tau_0}{F^b} e^{-a\alpha}, \tag{4.66}$$

where a and b are fitting parameters. Sturrock et al (1999) tried to use this approach to predict the permeability of eight sandstone cores with permeability ranging over three orders of magnitude. They found that τ_0 was not very sensitive to the mean pore/grain size for these samples, and that the permeability prediction was mainly controlled by the variations in F and α. More experiments on well-characterized samples are required to better test this approach to permeability prediction.

It is interesting to note the mathematical similarity between the Havriliak-Negami dielectric model (Equation 4.47) and the van Genuchten model for soil-moisture-retention curves (Equation 4.10). Both of these empirically derived functions can be theoretically related to the statistics of the grain- or pore-size distributions of the sample. It is possible that broadband dielectric measurements could eventually be used to predict the van Genuchten parameters for at least some types of materials. However, the dielectric response is also dependent upon the surface chemical properties of the sample (e.g., clay type and solution chemistry), so any predictive relationships that are established will have to account for these effects. Even if it is not possible to predict van Genuchten parameters from dielectric spectra, IP estimates of the effective pore or

grain size, as discussed in Section 4.5, could be helpful for characterizing the water-retention properties of rock and soil formations, especially if some core measurements are available to establish site-specific relationships.

4.7 Conclusions

Electrical methods are commonly used in hydrogeophysical investigations to characterize the lithologic properties of subsurface formations and to characterize and monitor the pore fluid saturation and salinity. The most commonly measured electrical parameters are the high-frequency permittivity and the low-frequency conductivity. Permittivity measurements can be used to estimate the porosity of fully saturated formations and the water content of partially saturated formations. Electrical conductivity measurements are sensitive to the water content, the water conductivity, and the lithology. Petrophysical relationships can be used to predict the electrical conductivity responses of rocks and soils in terms of these controlling parameters. The hydrological properties of subsurface formations can be estimated by performing dynamic experiments, such as permittivity monitoring of water infiltration tests in the vadose zone or conductivity monitoring of saline tracer tests in the saturated zone. However, direct estimates of the subsurface permeability structure from permittivity and conductivity measurements are generally not possible. The correlations used in the literature are very site specific, and there is a wide degree of scatter in the permeability predictions. The IP response, however, is strongly correlated with the effective clay content and the specific surface area of rocks and soils. Because the permeability is largely controlled by these lithologic parameters, IP measurements can be used in many cases to estimate subsurface permeability variations to within an order of magnitude. More accurate and robust IP-permeability prediction equations will need to account for the dependence of the IP response on the solution conductivity and saturation degree. This will require jointly measuring the IP, permittivity, and conductivity responses of subsurface formations and developing the appropriate petrophysical models.

The permittivity and conductivity responses of water-bearing rocks and soils also vary with frequency. The empirical Cole-Cole model can be used to fit the frequency-dependent permittivity and conductivity responses of rocks and soils with only five model parameters. Theoretically based effective media models can be used to interpret the Cole-Cole model parameters in terms of fundamental physical and chemical properties of the porous media. These models and laboratory data illustrate the important affect that the surface phase has on the frequency-dependent permittivity and conductivity responses of rocks and soils. More laboratory experiments are needed on well-characterized samples made as a function of frequency, solution chemistry, and saturation to better understand the polarization mechanisms operating within rocks and soils. These laboratory experiments and theoretical analyses should lead to a better understanding of the Cole-Cole type of empirical functions widely used to interpret and model electrical field surveys.

Lastly, the electrical methods and petrophysical models discussed in this chapter will be most effective when combined with other geophysical, geological, and hydrological

measurements and integrated using appropriate geostatistical and geological models, as is illustrated by other chapters in this volume.

4.8 Appendix: Electrical Properties of Aqueous Solutions

This appendix contains equations for computing the dielectric constant and electrical conductivity of aqueous solutions as a function of temperature and ionic concentration.

The dielectric constant of aqueous solutions decreases with increasing temperature and to a lesser degree with increasing ionic concentration. The temperature dependence of pure water is given by (Weast, 1983):

$$\kappa_w(t) = 78.54\left[1 - 4.759\times10^{-3}(t-25) + 1.19\times10^{-5}(t-25)^2 - 2.8\times10^{-8}(t-25)^3\right], \quad (4.67)$$

where t is in °C. The concentration dependence for mono valent aqueous solutions (e.g., LiCl and NaCl) is approximately given by Olhoeft (1981):

$$\kappa_w(c) = \kappa_w(t) - 13.00c + 1.065c^2 - 0.03006c^3, \quad (4.68)$$

where c is the effective salt concentration in moles per liter of solution.

Pure water has a very low electrical conductivity of $\sim 4\times10^{-6}$ S/m (Weast, 1983). The conductivity of natural waters containing dissolved salts and other ionic components is much larger with pore water conductivities ranging from ~0.01 S/m for freshwater aquifers to 20 S/m for oil field brines (e.g., Schön, 1996). The conductivity of an aqueous solution containing n ionic components is given by:

$$\sigma_w \cong \sum_{i=1}^{n} \alpha_i c_i z_i \mu_i, \quad (4.69)$$

where the parameters are ionic concentration (c_i), valence (z_i),ionic mobility (μ_i), and the degree of dissociation (α_i) (e.g., Schön, 1996; Weast, 1983). Empirical relationships can be used to relate the electrical conductivity of aqueous solutions to the total dissolved solids, or *TDS* (Fishman and Friedman, 1989):

$$\sigma_w(S/m) \cong a \times TDS(mg/L), \quad (4.70)$$

where, depending upon the ionic composition and temperature of the solution, the constant a can range from ~1.2x10^{-4} to ~2.0x10^{-4}. An average value of a=1.5x10^{-4} is typically used to predict the conductivity of natural waters at 25 degrees C (Fishman and Friedman, 1989)). The solution conductivity also increases with increasing temperature as the ionic mobility and the degree of dissociation are temperature dependent. The solution conductivity increases by ~2% per degree C increase in temperature for temperatures ranging between 20 and 30 degrees C. The temperature dependence of NaCl solutions is described by the following empirical equation (Arps, 1953):

$$\sigma_w(t_2) = \sigma_w(t_1)\frac{t_2 + 21.5}{t_1 + 21.5}, \tag{4.71}$$

where the temperature is in °C. A comprehensive set of equations for the electrical conductivity of NaCl solutions as a function of concentration and temperature was published by Worthington et al. (1990).

Acknowledgments

We thank Lee Slater for his helpful advice about the content and organization of this chapter and his insightful review of the manuscript. We also thank Susan Hubbard for her advice, encouragement and careful review of this chapter.

References

Alharthi, A., and J. Lange, Soil water saturation: Dielectric determination, *Water Resour. Res.*, *23*, 591–595, 1987.

Amente, G., J.M. Baker, and C.F. Reece, Estimation of soil solution electrical conductivity from bulk soil electrical conductivity in sandy soils, *Soil. Sci. Soc. Am. J., 64,* 1931–1939, 2000.

Archie, G.E., The electrical resistivity log as an aid in determining some reservoir characteristics, *Trans. Amer. Inst. Mining Metallurgical and Petroleum Engineers*, *146*, 54–62, 1942.

Arps, J.J., The effect of temperature on the density and electrical resistivity of sodium chloride solutions, *Trans. AIME*, *198*, 327, 1953.

Bernabé, Y., and A. Revil, Pore-scale heterogeneity, energy dissipation and the transport properties of rocks, *Geophys. Res. Lett.*, *22,* 1529–1232,1995.

Birchack, J.R., C.G.Z. Gardner, J.E. Hipp, and J.M. Victor, High dielectric constant microwave probes for sensing soil moisture, *Proc. IEEE*, *62,* 93–98, 1974.

Börner, F.D., and J.H. Schön, A relation between the quadrature component of electrical conductivity and the specific surface area of sedimentary rocks, *The Log Analyst*, *32,* 612–613, 1991.

Börner, F.D., J.R. Schopper, and A. Weller, Evaluation of transport and storage properties in the soil and groundwater zone from induced polarization measurements, *Geophysical Prospecting*, *44,* 583–602, 1996.

Böttcher, C.J.F., and P. Bordewijk, *Theory of Electric Polarization, Vol II*, Elsevier Sci., New York, 1978.

Bruggeman, D.A.G., The calculation of various physical constants of heterogeneous substances: I. The dielectric constants and conductivities of mixtures composed of isotropic substances, *Ann. Phys., 24,* 636–664, 1935.

Bussian, A.E., Electrical conductance in a porous medium, *Geophysics*, *49,* 1258–1268, 1983.

Carman, P.C., Permeability of saturated sands, soils and clays, *J. Agric. Sci*., *29,* 262–273, 1939.

Chelidze, T.L., and Y. Gueguen, Electrical spectroscopy of porous rocks: a review- I. Theoretical models, *Geophys. J. Int*., *137,* 1–15, 1999.

Chelidze, T.L., Y. Gueguen, and C. Ruffet, C., 1999, Electrical spectroscopy of porous rocks: a review- II. Experimental results and interpretation, *Geophys. J. Int*., *137,* 16–34, 1999.

Chen, J., S. Hubbard, and Y. Rubin, Estimating the hydraulic conductivity at the South Oyster Site from geophysical tomographic data using Bayesian techniques based on the normal linear regression model, *Water Resour. Res.*, *37,* 1603–1613, 2001.

Chew, W.C., and P.N. Sen, Dielectric enhancement due to electrochemical double layers: Thin double layer approximation, *J. Chem. Phys., 77,* 4683–4693, 1982.

Cole, K.S., and R.H. Cole, Dispersion and adsorption in dielectrics, I, Alternating current characteristics, *J. Chem. Phys.*, *9,* 341–351, 1941.

Davidson, D. W., and R.H. Cole, Dielectric relaxation in glycerol, propylene glycol and n-propanol, *J. Chem. Phys*., *19,* 1484–1490, 1951.

de Kuijper, A., R.K.J. Sandor, J.P. Hofman, and J.A. de Waal, Conductivity of two-component systems. *Geophysics, 61,* 162–168, 1996.

de Lima, O.A.L., and S. Niwas, Estimation of hydraulic parameters of shaly sandstone aquifers from geoelectrical measurements, *Journal of Hydrology, 235*, 12–26, 2000.

de Lima, O.A.L., and M.M. Sharma, A generalized Maxwell-Wagner theory for membrane polarization in shaly sands, *Geophysics*, *57*, 431–440, 1992.

Dirksen, C., and S. Dasberg, Improved calibration of time domain reflectometry soil water content measurements, *Soil Sci. Soc. Am. J., 57*, 660–667, 1993.

Dobson, M.C., F. Kouyate, and F.T. Ulaby, A reexamination of soil textural effects on microwave emission and backscattering, *IEEE Trans. Geosc. Remote Sensing, GE-22*, 530–536, 1984.

Dobson, M.C., F.T. Ulaby, M.T. Hallikainen, and M.A. El-Rayes, Microwave dielectric behavior of wet soil: II. Dielectric mixing models, *IEEE Trans. Geosc. Remote Sensing, GE-23*, 35–46, 1985.

Doyen, P.M., Permeability, conductivity, and pore geometry of sandstones, *J. Geophys. Res*., *93*, 7729–7740, 1988.

Endres, A.L., and R.J. Knight, A theoretical assessment of the effect of microscopic fluid distribution on the dielectric response of partially saturated rocks, *Geophysical Prospecting*, *40,* 307–324, 1992.

Feng, S., and P.N. Sen, Geometrical model of conductive and dielectric properties of partially saturated rocks, *J. Appl. Phys*., *58*, 3236–3243, 1985.

Fetter, C.W*., Applied Hydrogeology*, 4th ed., Prentice Hall, Upper Saddle River, NJ, 2001.

Fishman, M. J., and Friedman, L. C., Methods of determination of organic substances in water and fluvial sediments, *Techniques of Water-Resource Investigations of the U.S. Geological Survey, book 5, chapter A1.,* 1989.

Friedman, S.P., Statistical mixing model for the apparent dielectric constant of unsaturated porous media, *Soil Sci. Soc. Am. J., 61,* 742–745, 1997.

Friedman, S.P., A saturation degree-dependent composite spheres model for describing the effective dielectric constant of unsaturated porous media, *Water Resour. Res*., *34,* 2949–2961, 1998a.

Friedman, S.P., Simulation of a potential error in determining soil salinity from measured apparent electrical conductivity, *Soil Sci. Soc. Am. J., 62,* 593–599, 1998b.

Friedman, S.P., and D.A. Robinson, Particle shape characterization using angle of repose measurements for predicting the effective permittivity and electrical conductivity of saturated granular media, *Water Resour. Res., 38,* doi:10.1029/2001WR000746, 2002.

Friedman, S.P., and N.A. Seaton, Critical path analysis of the relationship between permeability and electrical conductivity of 3-dimensional pore networks, *Water Resour. Res., 34,* 1703–1710, 1998.

Glover, P.W.J., P.G. Meredith, P.R. Sammonds, and S.A.F. Murrel, Ionic surface electrical conductivity in sandstone, *J. Geophys. Res.*, *99,* 21635–21650, 1994.

Hanai, T., Theory of the dielectric dispersion due to the interfacial polarization and its applications to emulsions, *Kolloid Z., 171,* 23–31, 1960.

Havriliak, S., and S. Negami, A complex plane analysis of α—dispersion in some polymer systems in transition and relaxations in polymers, *J. Polymer Sci.,* Part C Polym. Lett., *14,* 99–117, 1966.

Heigold, P.C., R.H. Gilkeson, K. Cartwright, and P.C. Reed, Aquifer transmissivity from surficial electrical methods, *Ground Water*, *17,* 338–345, 1979.

Heimovaara, T. J., Frequency domain analysis of time domain reflectometry waveforms, 1, Measurements of complex dielectric permittivity of soils, *Water Resour. Res., 30,* 189–199, 1994.

Hubbard, S.S., Y. Rubin, and E. Majer, Ground-penetrating-radar assisted saturation and permeability estimation in bimodal systems. *Water Resour. Res. 33***,** 971–990, 1997.

Hubbard, S.S., Y. Rubin, and E. Majer, Spatial correlation structure estimation using geophysical and hydrological data. *Water Resour. Res., 35,* 1809–1825, 1999.

Huntley, D., 1986, Relations between permeability and electrical resistivity in granular aquifers, *Ground Water*, *24,* 466–474, 1986.

Jackson, P.D., D.T. Smith, and P.N. Stanford, Resistivity-porosity-particle shape relationships for marine sands, *Geophysics*, *43,* 1250–1268, 1978.

Jacobsen, O.H., and P. Schjonning, A laboratory calibration of time domain reflectometry for soil water measurement including effects of bulk density and texture, *J. Hydrol.*, *151,* 147–157, 1993.

Johnson, D.L., J. Koplik, and L.M. Schwartz, New pore-size parameter characterizing transport in porous media, *Phys. Rev. Lett.*, *57,* 2564–2567, 1986.

Johnson, I.A., Spectral induced polarization parameters as determined through time-domain measurements, Geophysics, *49,* 1993–2003, 1984.

Jones, S.B., and S.P. Friedman, Particle shape effects on the effective permittivity of anisotropic or isotropic media consisting of aligned or randomly oriented ellipsoidal particles. *Water Resour. Res*., *36,* 2821–2833, 2000.

Kemna, A., Tomographic inversion of complex resistivity – Theory and application, Ph.D. thesis, Bochm Univ. (published by: Der Andere Verlag, Osanabruck, Germany), 2000.
Kenyon, W.E., Texture effects on the megahertz dielectric properties of rock samples, *J. Appl. Phys., 55,* 3153–3159, 1984.
Klein, J.D., and W.R. Sill, Electrical properties of artificial clay-bearing sandstone, *Geophysics*, *47,* 1593–1605, 1982.
Kosugi, K., Three-parameter lognormal distribution model for soil water retention, *Water Resour. Res.*, *30,* 891–901, 1994.
Knight, R.J., and A. Nur, The dielectric constant of sandstones, 60 kHz to 4 MHz, *Geophysics*, *52,* 644–654, 1987a.
Knight, R. J., and A. Nur, Geometrical effects in the dielectric response of partially saturated sandstones, *The Log Analyst*, *28,* 513–519, 1987b.
Knight, R.J., Hysteresis in the electrical resistivity of partially saturated sandstones, *Geophsyics*, *56*, 2139–2147, 1991.
Knight, R. J., and A.L. Endres, A new concept in modeling the dielectric response of sandstones: Defining a wetted rock and bulk water system, *Geophysics*, *55,* 586–594, 1990.
Knoll, M.D., R. Knight, and E. Brown, Can accurate estimates of permeability be obtained from measurement of dielectric properties? Paper Presented at Symposium on the Application of Geophysics to Environmental and Engineering Problems, *Environ. and Eng. Geophys. Soc.*, Orlando, FL, April 23–26, 1995.
Kosinski, W.K. and W.E. Kelly, Geoelectric soundings for predicting aquifer properties, *Ground Water*, *19*, 163–171, 1981.
Lesmes, D.P., and K.M. Frye, The influence of pore fluid chemistry on the complex conductivity and induced polarization responses of Berea sandstone, *J. Geophys. Res., 106,* 4079–4090, 2001.
Lesmes, D.P., and F.D. Morgan, Dielectric spectroscopy of sedimentary rocks, *J. Geophy. Res*., *106,* 13,329–13,346, 2001.
Lesmes, D.P., J. Sturrock, and K.M. Frye, A physicochemical interpretation of the Cole-Cole dielectric model, *Proceedings of the Symposium on the Application of Geophysics to Environmental and Engineering Problems (SAGEEP),* Environ. and Eng. Geophys. Soc., Arlington, VA, 2000.
Looyenga, H., Dielectric constants of mixtures, *Physica*, *31,* 401–406, 1965.
Man, H.N., and X.D. Jing, Network modeling of strong and intermediate wettability on electrical resistivity and capillary pressure, *Adv. Water Resour.*, *24,* 345–363, 2001.
Marshall, D.J., and T.R. Madden, Induced polarization: A study of its causes, *Geophysics, 24,* 790–816, 1959.
Maxwell-Garnett, J.C., Colours in metal glasses and in metal films, *Trans. R. Soc. London*, *203,* 385–420, 1904.
Mendelson, K.S., and M.H. Cohen, The effect of grain anisotropy on the electrical properties of sedimentary rocks, *Geophysics 47,* 257–263, 1982.
Morgan, F.D., and D.P. Lesmes, Inversion for dielectric relaxation spectra, *J. Chem. Phys*., *100,* 671–681, 1994.
Mualem, Y., A new model for predicting the hydraulic conductivity of unsaturated porous media, *Water Resour. Res.*, *12,* 513–522, 1976.
Mualem, Y., and S.P. Friedman, Theoretical prediction of electrical conductivity in saturated and unsaturated soil, *Water Resour. Res.*, *27,* 2771–2777, 1991.
Nadler, A., Estimating the soil water dependence of the electrical conductivity soil solution/electrical conductivity bulk soil ratio, *Soil Sci. Soc. Am. J.*, *46,* 722–726, 1982.
Nelson, P.H., Permeability-porosity relationships in sedimentary rocks, *The Log Analyst, 35,* 38–61, 1994.
Olhoeft, G.R., Electrical properties of rocks. In *Physical Properties of Rocks and Minerals*, Y.S. Touloukian and C.Y. Ho, eds., McGraw-Hill / CINDAS Data Series on Material Properties, Volume II-2, pp. 298–329, McGraw-Hill book company, New York, 1981.
Olhoeft, G.R., Low-frequency electrical properties, *Geophysics, 50,* 2492–2503, 1985.
Olhoeft, G.R., Electrical properties from 10^{-3} to 10^{9} Hz- physics and chemistry, in *Physics and Chemistry of Porous Media, II,* J.R. Banavar, J. Koplik, and K. W. Winkler, eds., *AIP Conf. Proc., 154*, pp. 775–786, 1986.
Or, D., and J.M. Wraith, Temperature effects on soil bulk dielectric permittivity measured by time domain reflectometry: A physical model, *Water Resour. Res.*, *35,* 371–383, 1999.
Pelton, W.H., S.H. Ward, P.G. Hallof, W.R. Sill, and P.H. Nelson, Mineral discrimination and removal of inductive coupling with multifrequency IP, *Geophysics*, *43,* 588–609, 1978.

Pengra, D.B., and P.Z. Wong, Low-frequency AC electrokinetics, *Colloids & Surf. A: Physicochem. Eng. Aspects, 159,* 283–292, 1999.
Polder, D., and J.H. van Santen, The effective permeability of mixtures of solids, *Physica*, *12,* 257–271, 1946.
Purvance, D.T., and R. Andricevic, On the electrical-hydraulic conductivity correlation in aquifers, *Water Resour. Res., 36,* 2905–2913, 2000.
Revil, A., and L.M. Cathles, Permeability of shaly sands, *Water Resour. Res.*, *35,* 651–662, 1999.
Revil, A., and P.W.J. Glover, Theory of ionic-surface electrical conduction in porous media, *Phys. Rev. B.*, *55,* 1757–1773, 1997.
Revil, A., D. Hermitte, E. Spangenberg, and J.J. Cocheme, Electrical properties of zeolitized volcaniclastic materials. *J. Geophys. Res*., *107,* doi:10.1029/2001JB000599, 2002.
Rhoades, J.D., P.A.C. Ratts, and R.J. Prather, Effects of liquid-phase electrical conductivity, water content, and surface conductivity on bulk soil electrical conductivity, *Soil Sci. Soc. Am. J.*, *40,* 651–655, 1976.
Rink, M., and J.R. Schopper, Interface conductivity and its implications to electric logging, *Trans. 15th Ann. Logging Symp., Soc. Prof. Well Log Analysts*, 1–15, 1974.
Roberts, J.J., and W. Lin, Electrical properties of partially saturated Topopah Spring tuff: Water distribution as a function of saturation, *Water Resour. Res*., *33,* 577–587, 1997.
Robinson, D.A., Measurement of the solid dielectric permittivity of clay minerals and granular samples using time domain reflectometry immersion method, *Vadose Zone J., 3,* 705–713, 2004.
Robinson, D.A., and S.P. Friedman, The effect of particle size distribution on the effective dielectric permittivity of saturated granular media, *Water Resour. Res.*, *37,* 33–40, 2001.
Robinson, D.A., and S.P. Friedman, The effective permittivity of dense packings of glass beads, quartz sand and their mixtures immersed in different dielectric background, *J. Non-Crystaline Solids*, *305,* 261–267, 2002.
Robinson, D.A., and S.P. Friedman, A method for measuring the solid particle permittivity or electrical conductivity of rocks, sediments, and granular materials, *J. Geophys. Res.*, *108*(B2), 2075, doi:10.1029/2001JB000691, 2003.
Robinson, D.A., C.M.K. Gardner, and J.D. Cooper, Measurement of relative permittivity in sandy soils using TDR, capacitance and theta probes: comparison, including the effects of bulk soil electrical conductivity, *J. Hydrol., 223,* 198–211, 1999.
Roth, C. H., M.A. Malicki, and R. Plagge, Empirical evaluation of the relationship between soil dielectric constant and volumetric water content as the basis for calibrating soil moisture measurements by TDR, *J. Soil Sci., 43,*1–13, 1992.
Roth, K., R. Schulin, H. Fluhler, and W. Attinger, Calibration of time domain reflectometry for water content measurement using a composite dielectric approach, *Water Resour. Res.*, *26,* 2267–2273, 1990.
Ruffet, C., Y Gueguen, and M. Darot, Complex measurements and fractal nature of porosity, *Geophysics*, *56,* 758–768, 1991.
Samstag, F. J., and F.D. Morgan, Induced polarization of shaly sands: Salinity domain modeling by double embedding of the effective medium theory, Geophysics, *56,* 1749–1756, 1991.
Samstag, F. J., An effective-medium model for complex conductivity of shaly sands in the salinity, frequency, and saturation domains, Ph.D. Thesis, Texas A&M Univ., College Station, TX, 1992.
Scheidegger, A.E., *The Physics of Flow through Porous Media*, Toronto: University of Toronto Press, 1974.
Schön, J.H., Physical properties of rocks – fundamentals and principles of petrophysics, Elsevier Science Ltd., *Handbook of Geophysical Exploration, Seismic Exploration, 18*, 379–478, 1996.
Schwartz, L.M., and S. Kimminau, Analysis of electrical conduction in the grain consolidated model, *Geophysics, 52,* 1402–1411, 1987.
Schwartz, L.M., P.N. Sen, and D.L. Johnson, Influence of rough surfaces on electrolyte conduction in porous media, *Phys. Rev. B.*, *40,* 2450–2458, 1989.
Schwarz, G., A theory of the low-frequency dielectric dispersion of colloidal particles in electrolyte solution, *J. Phys. Chem.*, *66,* 2636–2642, 1962.
Scott, J.B.T., and R.D. Barker, Determining pore-throat size in Permo-Triassic sandstones from low-frequency electrical spectroscopy, *Geophys. Res. Lett.*, *30*(9), 1450, doi:10.1029/2003GL016951, 2003.
Sen, P.N., C. Scala, and M.H. Cohen, A self-similar model for sedimentary rocks with application to the dielectric constant of fused glass beads. *Geophysics*, ***46,*** 781–795, 1981.
Sen, P.N., Grain shape effects on dielectric and electrical properties of rocks, *Geophysics, 49,* 586–587, 1984.
Sen, P.N., P.A. Goode, and A. Sibbit, Electrical conduction in clay bearing sandstones at low and high salinities, *J. Appl. Phys.*, *63,* 4832–4840, 1988.
Sihvola, A., and J.A. Kong, Effective permittivity of dielectric mixtures, *IEEE Trans. Geosci. Remote Sens.,*

26, 420–429, 1988.
Sihvola, A., and J.A. Kong, Correction to "Effective permittivity of dielectric mixtures," *IEEE Trans. Geosci. Remote Sens., 21,* 101–102, 1989.
Slater, L., and D.P. Lesmes, IP Interpretation in environmental investigations, *Geophysics*, *67,* 77–88, 2002a.
Slater, L., and D.P. Lesmes, Electrical-hydraulic relationships observed for unconsolidated sediments, *Water Resour. Res*., *38*(10), 1213, doi:10.1029/2001WR001075, 2002b.
Sturrock, J.T., D.P. Lesmes, and F.D. Morgan, Permeability estimation using spectral induced polarization measurements, Paper presented at the Symposium on the Application of Geophysics to Environmental and Engineering Problems (SAGEEP*)*, *Environ. Eng. Geophys. Soc.*, Oakland, CA, 1999.
Titov, K., V. Komarov, V. Tarasov, and A. Levitski, Theoretical and experimental study of time domain-induced polarization in water-saturated sands, *J. Appl. Geophys*., *50,* 417–433, 2002.
Topp, G.C., J.L. Davis, and A.P. Annan, Electromagnetic determination of soil water content: Measurements in coaxial transmission lines, *Water Resour. Res.*, *16,* 574–582, 1980.
Tsang, L., J.A. Kong, and R.T. Shin, *Theory of Microwave Remote Sensing*, John Wiley, New York, 1985.
Ulrich, C., and L. Slater, Induced polarization measurements on unsaturated sands, *Geophysics*, *69,* 762–771, 2004.
Van Genuchten, M.T., A closed-form equation for predicting the hydraulic conductivity of unsaturated soils, *Soil Sci. Soc. Am. J.*, *44,* 892–898, 1980.
Vanhala, H., and H. Soininen, Laboratory technique for measurement of spectral induced polarization soil samples, *Geophysical Prospecting*, *43,* 655–676, 1995.
Vinegar, H.J., and M.H. Waxman, Induced polarization of shaly sands, *Geophysics, 49,* 1267–1287, 1984.
Ward, S.H., Resistivity and Induced Polarization Methods, in *Geotechnical and Environmental Geophysics*, Vol. 1, *Review and Tutorial*, *Invest. Geophys. 5,* S.H. Ward, ed., pp. 141–190, Soc. of Explor. Geophys., Tulsa, OK, 1980.
Wang, J.R., and T.J. Schmugge, An empirical model for the complex dielectric constant of soils as a function of water content, *IEEE Trans. Geosci. Remote Sensing*, *GE-18*, 288–295, 1980.
Waxman, M.H., and L.J.M. Smits, Electrical conductivities in oil-bearing shaly sands, *Soc. Pet. Eng. J.*, *8,* 107–122, 1968.
Weast, R.C., ed., *CRC Handbook of Chemistry and Physics* (63rd edition), CRC Press, Inc., Boca Raton, Florida, 1983.
Weerts, A. H., W. Bouten, and J.M. Verstraten, Simultaneous measurement of water retention and electrical conductivity in soils: Testing the Mualem-Friedman tortuosity model, *Water Resour. Res.*, *35,* 1781–1787, 1999.
Wharton, R.P., G.A. Hazen, R.N. Rau, and D.L. Best, Electromagnetic propagation logging: Advances in technique and interpretation, *Soc. Pet. Eng.*, *Pap. No. 9267,* 1980.
Wong, J., An electrochemical model of the induced-polarization phenomenon in disseminated sulfide ores, *Geophysics*, *44,* 1245–1265, 1979.
Worthington, A.E., J.H. Hedges, and N. Pallatt, SCA guidelines for sample preparation and porosity measurement of electrical resistivity samples: Part I–Guidelines for preparation of brine and determination of brine resistivity for use in electrical resistivity measurements, *The Log Analyst, 31,* 20, 1990.
Wyllie, M.R.J., and A.R. Gregory, Fluid flow through unconsolidated porous aggregates: Effect of porosity and particle shape on Kozeny-Carman constants, *Indust. Eng. Chem*, *47,* 1379–1388, 1955.